National Library of Canada
Acquisitions and Bibliographic Services Branch
395 Wellington Street
Ottawa, Ontario
K1A 0N4

Bibliothèque nationale du Canada
Direction des acquisitions et des services bibliographiques
395, rue Wellington
Ottawa (Ontario)
K1A 0N4

Your file Votre référence

Our file Notre référence

NOTICE

The quality of this microform is heavily dependent upon the quality of the original thesis submitted for microfilming. Every effort has been made to ensure the highest quality of reproduction possible.

If pages are missing, contact the university which granted the degree.

Some pages may have indistinct print especially if the original pages were typed with a poor typewriter ribbon or if the university sent us an inferior photocopy.

Reproduction in full or in part of this microform is governed by the Canadian Copyright Act, R.S.C. 1970, c. C-30, and subsequent amendments.

AVIS

La qualité de cette microforme dépend grandement de la qualité de la thèse soumise au microfilmage. Nous avons tout fait pour assurer une qualité supérieure de reproduction.

S'il manque des pages, veuillez communiquer avec l'université qui a conféré le grade.

La qualité d'impression de certaines pages peut laisser à désirer, surtout si les pages originales ont été dactylographiées à l'aide d'un ruban usé ou si l'université nous a fait parvenir une photocopie de qualité inférieure.

La reproduction, même partielle, de cette microforme est soumise à la Loi canadienne sur le droit d'auteur, SRC 1970, c. C-30, et ses amendements subséquents.

Canada

UNIVERSITY OF ALBERTA

# Nonlinear Response of an Articulated Offshore Tower

by

Yan Wang

©

A thesis

submitted to the Faculty of Graduate Studies and Research

in partial fulfilment of the requirements for the degree of

Master of Science

in

Department of Mechanical Engineering

Edmonton, Alberta

Fall, 1993

National Library of Canada

Acquisitions and Bibliographic Services Branch

395 Wellington Street
Ottawa, Ontario
K1A 0N4

Bibliothèque nationale du Canada

Direction des acquisitions et des services bibliographiques

395, rue Wellington
Ottawa (Ontario)
K1A 0N4

Your file Votre référence

Our file Notre référence

**The author has granted an irrevocable non-exclusive licence allowing the National Library of Canada to reproduce, loan, distribute or sell copies of his/her thesis by any means and in any form or format, making this thesis available to interested persons.**

**L'auteur a accordé une licence irrévocable et non exclusive permettant à la Bibliothèque nationale du Canada de reproduire, prêter, distribuer ou vendre des copies de sa thèse de quelque manière et sous quelque forme que ce soit pour mettre des exemplaires de cette thèse à la disposition des personnes intéressées.**

**The author retains ownership of the copyright in his/her thesis. Neither the thesis nor substantial extracts from it may be printed or otherwise reproduced without his/her permission.**

**L'auteur conserve la propriété du droit d'auteur qui protège sa thèse. Ni la thèse ni des extraits substantiels de celle-ci ne doivent être imprimés ou autrement reproduits sans son autorisation.**

ISBN 0-315-88142-9

Canada

UNIVERSITY OF ALBERTA

# RELEASE FORM

Name of author : Yan Wang

Title of thesis : Nonlinear Response of an Articulated Offshore Tower

Degree : Master of Science

Year of this degree granted : Fall, 1993

Permission is hereby granted to the University of Alberta Library to produce single copies of this thesis and to lend or sell such copies for private, scholarly or scientific research purposes only.

The author reserves all other publication and other rights in association with the copyright in the thesis, and except as hereinbefore provided neither the thesis nor any substantial portion thereof may be printed or otherwise reproduced in any material form whatever without the author's prior written permission.

Yan Wang

Yan Wang

Date: Aug. 9, 93

UNIVERSITY OF ALBERTA

FACULTY OF GRADUATE STUDIES AND RESEARCH

The undersigned certify that they have read, and recommend to the Faculty of Graduate Studies and Research for acceptance, a thesis entitled:

**Nonlinear Response of an Articulated Offshore Tower**

submitted by **Yan Wang** in partial fulfilment of the requirements for the degree of Master of Science.

A. W. Lipsett (Supervisor)

W. H. Finlay

K. Nandakumar

Date: Aug. 3, 93

# Abstract

A single-degree-of-freedom model of an articulated tower with regular harmonic wave excitation is studied in this thesis. Of particular interest are the various nonlinearities which may influence the response. Specifically, the nonlinearity in the drag force and the nonlinearity in the expression for the fluid particle acceleration are given special consideration.

Three different forms of fluid particle acceleration are used in the appropriate expression for the wave kinematics. One of these is simply the local fluid particle acceleration which does not introduce a nonlinearity to the equation of motion. The use of this form of fluid particle acceleration allows the effect of the drag force nonlinearity to be considered independently. The other two forms of fluid particle acceleration include the local as well as the convective acceleration terms and it is the convective terms which contain the nonlinearity. It was found that this nonlinearity significantly influences the response of an articulated tower.

An Adams-Bashforth-Moulton numerical method is used to integrate the equations of motion of the articulated tower for a wide variety of system parameters. Numerical integration is necessary in this case due to the complicated form of nonlinearities present which means that analytical solutions are not available. Results indicate that the response of an articulated tower subjected to the excitation of regular harmonic waves depends significantly on the system parameters and shows a wide range of nonlinear behaviour. In particular, subharmonic response is a common phenomenon. As well a period doubling route to chaotic response was also observed for the case of large wave height and small drag coefficient. Coexistence of multiple competing solutions and jump phenomena were also identified for certain ranges of system parameters.

# Acknowledgements

I wish to thank my supervisor, Dr. A. W. Lipsett, for his guidance, advice, and assistance in the preparation of this thesis.

I also wish to express my deep gratitude to my husband, Yuan, for his understanding, encouragement and patience, to my son, Jia, who has added joy and sunshine to my life.

# Contents

**Chapter 1**

**Introduction** **1**

**Chapter 2**

**Literature Review** **6**

2.1 Wave Description and Sea States . . . . . 7

2.2 Wave Loading . . . . . 9

2.3 Review of Nonlinear Dynamics of Offshore Structures . . . . . 13

2.4 Useful Tools of Nonlinear Dynamic Analysis . . . . . 17

2.4.1 Poincaré Section . . . . . 18

2.4.2 Liapunov Exponents . . . . . 19

2.4.3 Fourier Spectrum . . . . . 21

**Chapter 3**

**Formulation of Equations of Motion** **23**

3.1 Linear Wave Theory . . . . . 24

3.2 Morison Equation . . . . . 25

3.3 Equations of Motion of Articulated Offshore Tower . . . . . 27

**Chapter 4**

**Response of an Articulated Tower** **34**

4.1 System Parameters . . . . . 36

4.2 Comparison of Solutions of Equations . . . . . 40

4.3 Frequency Response . . . . . 45

4.4 Subharmonic Response . . . . . 57

4.5 Bifurcation to Chaos . . . . . 65

4.6 Numerical Calculation of Liapunov Exponent . . . . . 73

**Chapter 5**

**Summary and Conclusions** **78**

**References** **82**

**Appendix A**

**Solutions Using Local Acceleration Only** **86**

**Appendix B**

**Numerical Calculation of the Largest Liapunov Exponent** **90**

B.1 Definition . . . . . 90

B.2 Algorithm for Computing the Largest Liapunov Exponent $\lambda_1$ . . . . 92

# List of Tables


4.1 Solutions for $D = 5m$ using $DU/Dt = \partial U/\partial t + U\partial U/\partial x$ . . . . . 58
4.2 Solutions for $D = 1m$ using $DU/Dt = \partial U/\partial t + U\partial U/\partial x$ . . . . . 59
4.3 Solutions for $D = 3m$ using $DU/Dt = \partial U/\partial t + U\partial U/\partial x$ . . . . . 60

A.1 Solutions for $D = 5m$ using $DU/Dt = \partial U/\partial t$ . . . . . 87
A.2 Solutions for $D = 3m$ using $DU/Dt = \partial U/\partial t$ . . . . . 88
A.3 Solutions for $D = 1m$ using $DU/Dt = \partial U/\partial t$ . . . . . 89

# List of Figures


3.1 Model of the articulated tower system . . . . . 28

4.1 Frequency response of the tower using local and total acceleration . 42
4.2 Comparison of the tower response using total acceleration . . . . . 44
4.3 Comparison of the tower response using total acceleration . . . . . 46
4.4 Comparison of the tower response using total acceleration . . . . . 47
4.5 Frequency response for different values of $C_d$ . . . . . 49
4.6 Frequency response for different values of $H$ . . . . . 50
4.7 Frequency response for different values of $d$ . . . . . 52
4.8 Frequency response for different values of $\beta$ . . . . . 55
4.9 Frequency response for different values of $D$ . . . . . 56
4.10 Two coexisting $n = 3$ solutions . . . . . 61
4.11 Period halving bifurcation . . . . . 63
4.12 Basins of attraction . . . . . 64
4.13 Bifurcation diagram . . . . . 67
4.14 Poincaré maps and power spectra . . . . . 68
4.15 Poincaré map and power spectrum for chaotic response . . . . . 72
4.16 Partial enlargement of bifurcation diagram . . . . . 74
4.17 Time evolution of the largest nonzero Liapunov exponent . . . . . 76

B.1 Calculation of the largest Liapunov exponent from time series . . . 91

# Notation

| | | |
|---|---|---|
| $A$ | – | amplitude of the fluid particle displacement |
| $B$ | – | buoyancy center of the tower |
| $C$ | – | structural damping coefficient |
| $C_a$ | – | added mass coefficient |
| $C_d$ | – | drag coefficient |
| $C_m$ | – | inertia coefficient |
| $D$ | – | diameter of the structure |
| $DU/Dt$ | – | total fluid particle acceleration in the direction of structure motion |
| $F$ | – | total fluid force per unit length of the structure given by the Morison equation |
| $F_B$ | – | buoyancy force of the tower |
| $F_I$ | – | fluid inertia force per unit length of the structure |
| $F_d$ | – | drag force per unit length of the structure |
| $F_D$ | – | total drag force acting on the tower |
| $G$ | – | mass center |
| $I$ | – | moment of inertia of the tower about its base |
| $I_a$ | – | added mass moment of inertia of tower about its base |
| $I_d$ | – | integral of the drag force term |
| $\mathbf{J}$ | – | Jacobian matrix |
| $H$ | – | wave height |
| $K_c$ | – | Keulegan-Carpenter number |
| $K_\lambda$ | – | coefficient, $K_\lambda = 1/(kD)/(kd)^2$ |
| $K_\varepsilon$ | – | coefficient, $K_\varepsilon = (kd-1)/(kd)^2$ |
| $K'_\varepsilon$ | – | coefficient, $K'_\varepsilon = 1/(kd)^2$ |
| $L$ | – | wave length |
| $L_B$ | – | distance from buoyancy center to tower base |
| $L_W$ | – | distance from mass center to the tower base |

$M(\theta, \dot{\theta}, t)$ – moment of the total fluid forces about the tower base
$R_e$ – Reynolds number
$R(\theta)$ – restoring moment about the tower base
$S_{\theta\theta}$ – power spectrum of the tower angular displacement
$T$ – wave period
$U$ – fluid particle velocity in the direction of the tower motion
$U_m$ – velocity amplitude of the flow
$\partial U/\partial t$ – local acceleration of fluid particle
$W$ – total tower weight

$d$ – water depth
$d_i(t_i)$ – evolved divergence of nearby phase trajectories at time $t_i$
$d_{0i}(t_{i-1})$ – initial divergence of nearby phase trajectories at time $t_{i-1}$
$d_i(t)$ – length of the $i^{th}$ ellipsoidal principal axis
$d(t)$ – the largest length of ellipsoidal principal axis at time $t$
$\mathbf{f}(\mathbf{x}, t)$ – nonlinear functions
$g$ – gravitational acceleration
$g(\theta, \dot{\theta}, t)$ – nonlinear function
$g_1(\theta, \dot{\theta}, t)$ – nonlinear function
$g_2(\theta, \dot{\theta}, t)$ – nonlinear function
$k$ – wave number
$l$ – distance from tower base to the infinitesimal element $dl$
$s$ – nondimensional distance along tower, $s = kl$
$t$ – time
$t_0, t_N$ – initial and final times used to calculate the Liapunov exponent
$u$ – horizontal component of the fluid particle velocity, $u = (\pi H/T)e^{s-kd}\cos(s\theta - \omega_f t)$
$u^*$ – function, $u^* = (kH/2)e^{(s-kd)}\cos\omega_f t$
$u^{**}$ – function, $u^{**} = (kH/2)e^{(s-kd)}\cos(s\theta - \omega_f t)$
$v$ – vertical component of the fluid particle velocity, $v = (\pi H/T)e^{s-kd}\sin(s\theta - \omega_f t)$
$x, \dot{x}, \ddot{x}$ – horizontal displacement, velocity, and acceleration of the tower
$\mathbf{x}$ – vector in phase space
$\mathbf{x}^*(t)$ – reference solution for a set of first order nonlinear equations $\dot{\mathbf{x}} = \mathbf{f}(\mathbf{x}, t)$
$\Delta\mathbf{x}(0, t_k)$ – initial divergence vector at $k^{th}$ time increment
$\Delta\mathbf{x}(\tau, t_k)$ – final divergence vector at $k^{th}$ time increment
$z$ – vertical coordinate

| | | |
|---|---|---|
| $\beta$ | – | system parameter which measures the ratio of the tower weight to the weight of water displaced by the tower |
| $\omega_n$ | – | natural frequency of the tower in water |
| $\omega_f$ | – | wave frequency |
| $\omega_r$ | – | response frequency of the tower |
| $\delta$ | – | Feigenbaum number, $\delta = 4.66920...$ for logistic equation |
| $\delta_i$ | – | a sequence of numbers showing the convergence to Feigenbaum number $\delta$ |
| $\Delta\omega_{fi}$ | – | the width of frequency window associated with periodic solutions of order $i$ on bifurcation diagram |
| $\rho$ | – | sea water density |
| $\tau$ | – | Liapunov time step size |
| $\mu$ | – | system parameter, $\mu = C/(I + I_a)$ |
| $\lambda$ | – | system parameter, $\lambda = (I_a/(I_a + I))(C_d/(C_m - 1))(6g/(\pi d))$ |
| $\lambda_1$ | – | the largest Liapunov exponent |
| $\lambda_i$ | – | the Liapunov exponents |
| $\varepsilon$ | – | coefficient, $\varepsilon = (I_a/(I_a + I))(C_m/(C_m - 1))(3g/(2d))$ |
| $\theta, \dot{\theta}, \ddot{\theta}$ | – | angular displacement, velocity, and acceleration of tower |
| $\theta_P, d\theta_P/dt$ | – | Poincaré points of the solution |
| $\theta_o$ | – | mean response amplitude |

# Chapter 1

# Introduction

One of the major problems facing the offshore industry is the development of exploration and production facilities for natural resources in deeper waters. Lee [1] presents data showing the gradual increasing of water depth for offshore structures which indicates the progress of the offshore industry. Specifically, in 1947, the first steel platform was installed in open water, in $6m$ water depth off the Louisiana coast. From the $1950s$ to the early $1970s$, water depth for offshore structures increased from $30m$ to about $120m$ and in 1976 a pile-supported steel jacket-type platform was installed in $260m$ of water in the Santa Barbara Channel off California. By the year 1978, the water depth further increased to $312m$ when a fixed jacket structure was installed in the Gulf of Mexico. To meet this challenge, the technology of the platform design and the techniques of installation have advanced rapidly in the past few decades. Now the offshore industry has turned to flexible or compliant structures to reduce the cost which increases significantly with water depth. Examples of this new generation of offshore structure are tension leg platforms, guyed tower platforms, compliant tower platforms, articulated towers, and floating production systems. For example, in 1983 a guyed tower was installed in $305m$ of water in the Lena Field of the Gulf of Mexico; in 1987 a bi-articulated column was installed

in $167m$ of water on the Bouri field in the Mediterranean Sea; in 1988 a tension leg platform was installed in Green Canyon area of the Gulf of Mexico in a record water depth of $507m$. Several reviews of future problems facing the oil industry arising from the use of compliant offshore structures as well as the solutions to these problems are given by Thornton [2] and Patel [3]. New oil fields, such as the Marlim and Albacora fields have been found in deep water ranging from $600m$ to $1100m$ in Campos Basin, offshore Brazil. As a result many oil companies have initiated projects to investigate the application of compliant offshore structures in water depths up to $1500m$.

This new generation of offshore structures, characterized by very low natural frequency and large working displacement, creates new challenges for both engineers and researchers. Low natural frequencies, which may fall into the wave frequency range, imply that resonant response of these structures may be excited and large damage may occur. Successful compliant structure design depends upon a good understanding of the dynamic behaviour and accurate prediction of the response of such structures, and is key to safe, economic and efficient design.

There exists nonlinear interaction mechanisms between ocean waves and offshore structures which makes the dynamics of compliant offshore structures extremely complex. The wave force acting on a slender structure is a nonlinear function of both the structure motion and the wave kinematics. However, the motion of the structure is in turn determined by the wave forces. This is the so-called wave-structure interaction. Isaacson [4] has given a comprehensive review of the research on this topic. One of nonlinearities in this wave-structure interaction is the hydrodynamic drag force, which is due to the pressure gradient resulting from flow separation around a submerged structural member. This force is frequently modeled by an empirical equation depending quadratically on the relative velocity between the fluid and structure. Wave kinematics are another source of nonlinearity especially when nonlinear wave theories are used to give the wave properties in extreme sea

states. Nonlinearity also arises in wave kinematics even for the range in which linear wave theory is valid but for which the convective terms, variations of fluid velocities with respect to their spatial coordinates, cannot be neglected. These convective terms provide additional nonlinearity to the system. An example of such a case is when the motion of the structure is very large and the wave kinematics need to be computed at the displaced position of the structure. In addition to these, there are other possible nonlinearities. The flexible nature of the structure itself, the flexibility of cables in guyed compliant offshore structures and the interaction between structure and foundation may result in a nonlinear stiffness for these structures. These effects will not be considered here. The inherent nonlinearity of compliant offshore systems implies that the full range of nonlinear responses such as subharmonic, superharmonic, and chaotic responses as well as the stability problems may occur in these systems and is the focus of the research in this thesis.

In a linear single degree of freedom system with harmonic forcing, the period of response is always the same as that of the excitation and the response amplitude is linearly proportional to the exciting amplitude. However in nonlinear systems, as is well known, the response of the system can be subharmonic, superharmonic, even chaotic in addition to the more typical harmonic response. Under certain conditions two or more than two different motions can coexist, depending on the initial conditions.

The recently found chaotic motion [5] is a random-like response exhibited by a perfectly deterministic system and has been observed in many physical systems by both numerical simulations and physical experiments. Here the distinction has to be made between random and chaotic motions. Random motion can result from problems in which the input forces or system parameters are not known exactly but only have a statistical description. In contrast chaotic motion can result from those problems in which there are no random or unpredictable inputs or parameters and the system is completely deterministic. The main distinguishing feature of

chaotic motion is the sensitive dependence on initial conditions. Sensitivity to initial conditions means that small differences in initial conditions will result in large differences in the final response. As will be illustrated later this is a result of exponential divergence of nearby trajectories in phase space when the response of system becomes chaotic [5]. The significant implication here is that long term prediction of system behaviour in this case becomes impossible. Because of this unpredictability structural design should avoid the system parameter range where chaotic response may occur.

It is the intent of this thesis to investigate the nonlinear behaviour of an articulated tower subjected to the regular harmonic ocean wave excitation for a variety of tower geometries in deep water. The influence of various nonlinearities will also be studied. The aim of this thesis is to gain insight into the dynamic response of this structure, to explore the possibility of dynamic instability and chaotic motion, and to provide useful information for the design of these compliant structures.

Articulated towers are being designed and installed in many offshore areas. They are employed as mooring towers for oil tankers as well as for drilling and production operations. An articulated tower is usually pinned at seabed, and remains vertical due to its own buoyancy or the buoyancy of special modules. A simple and useful model of an articulated tower is a single-degree-of-freedom system in which the tower itself is taken as an uniform rigid cylinder. The dynamics of this system can be described by a single-degree-of-freedom which is the model used in this thesis. The equations of motion of the articulated tower are formulated by assuming that linear wave kinematics are applicable and that the fluid forces acting on the structure are given by the well known Morison equation [6]. The hydrodynamic drag force nonlinearity and the nonlinearities arising from the wave kinematics being computed at the deformed position of the tower will be investigated in this thesis. No attempt will be made to investigate the influence of other nonlinearities on the response of the articulated tower. The nonlinear wave kinematic terms arise from the use of either

form of total fluid particle acceleration expressions, $DU/Dt = \partial U/\partial t + U\partial U/\partial x$ or $DU/Dt = \partial U/\partial t + (U - \dot{x})\partial U/\partial x$, here $U$ is the velocity component of the fluid particle in the direction of the structure motion and $\dot{x}$ is the velocity component of the structure in the same direction. In order to compare the effects of these two nonlinearities on the behaviour of the system, the local acceleration expression $DU/Dt = \partial U/\partial t$ alone is also used so that in this case the nonlinear quadratic drag force is the only nonlinearity in the equation of motion.

The solutions of the various systems are obtained by numerically integrating the equation of motion for a large variety of system parameters to provide a comprehensive understanding of the behaviour of the compliant articulated tower. In order to investigate the response of real structures in regular waves, the system parameters typical for a real articulated tower are chosen.

An outline of the remaining parts of this thesis is as follows. Chapter Two is a review of literature relevant to the current research on the nonlinear dynamics of compliant offshore structures, including the ocean environment and hydrodynamic loading acting on the offshore structures. Also some useful tools for studying nonlinear dynamic problems as well as some universal features of chaotic systems are reviewed. The equation of motion of the articulated tower is then formulated in Chapter Three. Chapter Four includes the discussion of the results obtained from numerical simulations. The effects of different values of various system parameters on the system response are discussed and the possible route to chaos by period doubling is identified. To test the sensitivity of the system to initial conditions, the largest nonzero Liapunov exponent for some cases is computed. The calculated positive Liapunov exponent further verifies observed chaotic response. In addition, the solutions of various equations of motion are compared each other to identify the dominant nonlinearity of the system studied here. Finally a summary and conclusion of this work as well as the direction of future research are given in Chapter Five.

# Chapter 2

# Literature Review

The ocean is subjected to the action of large-scale environmental phenomena in the form of wind and results in waves and current. These phenomena directly influence the environmental loading on offshore structures. The fluid loading induced by waves is of importance as it is normally the largest environmental loading acting on offshore structures. When the dynamic response of flexible offshore structures in deep water to the harmonic wave excitation is considered, these systems are often characterized by a nonlinear restoring force, and a nonlinear hydrodynamic exciting force. The nonlinear restoring force includes the geometric nonlinearity. The hydrodynamic exciting force includes a quadratic drag force, representing the wave-structure interactions, and a wave induced inertia force. This inertia force, usually being harmonic, may include an extra combined parametric and external nonlinear convective excitation component when convective terms are included in fluid acceleration. Thus compliant offshore systems belong to a class of nonlinear systems with combined parametric and external excitation.

The dynamics of nonlinear systems has attracted significant attention in recent years due to the extremely complex behaviour exhibited by even very simple systems. Complex responses such as subharmonic and chaotic responses, which are

not encountered in linear systems, have been observed in various nonlinear dynamic systems and experiments. May in his landmark paper [7] has discussed dynamic features of the logistic equation, showing that even very simple systems can exhibit very complex behaviour. Moon [5] has discussed the nonlinear dynamics of many systems and performed experimental work on forced vibrations of a buckled beam and investigated many of the characteristics of chaotic motion. Thompson and Stewart [8] have published an excellent book on chaotic dynamics which includes an example of the complex response of an offshore structure. Recent research on the behaviour of compliant offshore structures has revealed that the response of these structures is very complex because of the inherent complex nonlinearities in these structures even for the very simple models [9, 10, 11].

In this chapter, we will review the descriptions of waves, and the methods to calculate the fluid forces acting on slender offshore structures. Also the current research on the complex behaviour of compliant offshore structures will be discussed. Some universal features of chaotic systems and useful tools used to study nonlinear dynamic problems will also be summarized here.

## 2.1 Wave Description and Sea States

In order to provide the kinematical properties of waves necessary for calculating the wave loading on the structure, various wave theories have been developed. Such wave theories allow a description of a wave in terms of the wave height, period, and water depth to be translated into the values of fluid velocity, acceleration and pressure at any point under the wave. This prescribes an adequate knowledge of the wave data. There are two distinct approaches, corresponding to either a regular or irregular sea state, to describe the wave parameters which are used as an "input" to the structural design.

The first approach is a deterministic method which is based on a design wave

specified to represent the extreme loading conditions in a long interval known as the return period. The design wave is usually specified by statistically choosing the wave height, period, and direction such that it gives the largest design loads on the structure during its expected life time. With this specified design wave, the use of a fluid loading calculation method, such as the Morison equation which will be discussed in Chapter 3, and the appropriate wave theory will give the fluid forces. This method is realistic from the design point of view against structural failure due to large waves. However, it does not permit fatigue damage to be considered in the design and for many offshore structures this so-called design wave may not be the worst loading case. Waves with smaller wave heights and special wave periods that excite the resonant motions may induce larger structural loadings than the highest design wave. They can be considered if required, however.

The second approach is a stochastic method which is based on the nominal loading conditions. In this method all the data for wave forecasting are presented in the form of a complete wave spectrum. The method uses the stochastic spectral analysis to determine the fatigue and dynamic response of structures. The drawback of the method is that it is valid only when the superposition principle is applicable.

In the deterministic approach, the wave loading model is based on the design wave approximated by long-crested regular waves with a single frequency component and therefore represents a regular, unidirectional sea state. In the stochastic approach, waves of different periods and heights are allowed to be superimposed on one another to form the wave spectrum. It actually describes an irregular sea state which closely approximates a real sea state. Although purely regular harmonic waves are rarely observed in nature, a study of them reveals certain basic concepts which are fundamental to wave motion as well as the response of offshore structures. In this thesis, only the response of the articulated tower in regular sea waves will be studied.

## 2.2 Wave Loading

Offshore structures are subjected to both steady and time dependent forces due to the action of winds, waves and currents. Of these, wave forces are usually the most significant for offshore structures. Waves account for most of the structural loading and, because they are time dependent, produce dynamic effects tending to increase the stresses.

The force on a submerged structure is a result of the hydrodynamic pressure exerted by the fluid around it. In the case of ideal inviscid fluid, the total fluid force acting on this structure is obtained by integrating this pressure around the structure surface. For a fixed circular cylinder in an accelerating flow, the component of this fluid force per unit length on the structure in the horizontal direction is given by (see for example, Sarpkaya and Isaacson [12])

$$F_I = \rho C_m \frac{\pi D^2}{4} \frac{\partial U}{\partial t} \tag{2.1}$$

where $\rho$ is the fluid density, $D$ is the diameter of cylinder, $C_m$ is the inertia coefficient, and $\partial U/\partial t$ is the local fluid particle acceleration in the horizontal direction. This force is often called the inertia force as it is due to the fluid acceleration.

Now consider the case of a fixed cylinder in a real fluid. The cylinder will also experience a resistance due to the separation of flow and the formation of wake behind the cylinder in addition to the fluid inertia force. This drag force, for a fixed cylinder, is usually given by (see for example, Sarpkaya and Isaacson [12])

$$F_d = \frac{1}{2} \rho C_d D U |U|, \tag{2.2}$$

in which $C_d$ is the drag coefficient, and $U$ is the velocity of fluid particle in the horizontal direction. Note that if the cylinder is not fixed, then the relative velocity between the fluid and cylinder is often used in Equation 2.2.

Based on the above discussion, the well known Morison equation [12] then assumes that the total fluid force on the cylinder can be obtained by simply adding

these two forces together, which gives

$$F = \rho C_m \frac{\pi D^2}{4} \frac{\partial U}{\partial t} + \frac{1}{2} \rho C_d D U |U|. \tag{2.3}$$

This is the original form of the Morison equation, valid only for fixed cylinders, with two empirical coefficients $C_m$ and $C_d$ determined by appropriate experiments.

For a cylinder moving in an unidirectional, two-dimensional, accelerating fluid, in this case the inertia force, due to the fluid inertia and the acceleration of the cylinder, and the drag force, due the relative velocity between the fluid and the cylinder, become

$$F_I = \rho C_m \frac{\pi D^2}{4} \left( \frac{DU}{Dt} - \ddot{x} \right) + \rho \frac{\pi D^2}{4} \ddot{x} \tag{2.4}$$

and

$$F_d = \frac{1}{2} \rho C_d D (U - \dot{x}) |U - \dot{x}| \tag{2.5}$$

respectively, where $\dot{x}$ and $\ddot{x}$ are the velocity and acceleration of cylinder in the horizontal direction, and $DU/Dt$ is the total fluid acceleration in the same direction.

For small body problems, in which the ratio of the lateral dimension of the structure to wave length is less than about 0.2, combining these two forces gives the relative velocity formulation of the Morison equation for a flexible cylinder in an accelerating fluid as

$$F = \rho C_m \frac{\pi D^2}{4} \frac{DU}{Dt} - \rho C_a \frac{\pi D^2}{4} \ddot{x} + \frac{1}{2} \rho C_d D (U - \dot{x}) |U - \dot{x}| \tag{2.6}$$

where $C_a$ is the added mass coefficient, with $C_m = C_a + 1$. For a cylinder moving in an uniformly accelerating flow, theoretically the added mass coefficient $C_a = 1$ (see for example, Sarpkaya and Isaacson [12]), so that the theoretical value of the inertia coefficient is $C_m = 2$. The first term on the right-hand side of Equation 2.6 represents the inertia force due to the total fluid acceleration; the second term is

the inertia force due to the motion of the cylinder; and the third term is the drag force due the relative velocity between the fluid and cylinder.

If the acceleration and velocity of the cylinder are small, that is $\ddot{x} \approx 0$ and $\dot{x} \approx 0$, by neglecting terms involving $\ddot{x}$ and $\dot{x}$ and letting $DU/Dt = \partial U/\partial t$, Equation 2.6 becomes identical with Equation 2.3 which is for the case of a fixed cylinder in an accelerating fluid.

Several reviews have been made in the area of wave forces and structure responses in the recent past. Sarpkaya and Isaacson [12] have reviewed the progress made in many aspects of wave interaction with offshore structures. Chakrabarti [13] has discussed the advancements made in this area, in particular, the various extensions and modifications of the Morison equation were discussed and their justifications investigated.

For large body problems in which the diffraction effect is important, that is the ratio of the lateral dimension of the structure to wave length is greater than 0.2, the hydrodynamic forces will include the fluid force component arising from this diffraction effect and the diffraction theory should be employed to predict the hydrodynamic forces. This effect is not considered here.

It should be mentioned that the inertia coefficient $C_m$ in Equation 2.4 and the drag coefficient $C_d$ in Equation 2.5 depend mainly on the Reynolds number $R_e$, defined as $R_e = U_m D/\nu$, and Keulegan-Carpenter number $K_c$, defined as $K_c = U_m T/D = 2\pi A/D$ which is proportional to the ratio of the fluid particle displacement to the cylinder diameter, where $U_m$ is the maximum fluid particle velocity, $A$ is the fluid particle displacement, $D$ is the structure diameter, $T$ is the wave period, and $\nu$ is the kinematic viscosity. Usually these two coefficients are determined from experiments by the method of Fourier averages as detailed by Keulegan and Carpenter [14]. The research in this field has suggested that they should be only determined by appropriate experiments and their values are strictly

applicable to the form of the Morison equation from which they are obtained. Reliable data of these two coefficients have been obtained for fixed body problems by the work of many researchers. However, for the case of a body moving in waves the experimental data is rare. A good review on this topic is given by Sarpkaya and Isaacson [12]. An attempt to investigate this area was also made by Chakrabarti and Cotter [15]. Their tests showed that the relative velocity form of the Morison equation is generally applicable. The work by Williamson [16] has also indicated above conclusion except for a small region near the first resonance in which the two force coefficients $C_m$ and $C_d$ for flexible cylinders depart significantly from those for fixed cylinders. Koterayama and Nakamura [17] have also investigated the validity of relative velocity form of the Morison equation. It was shown from their work that the relative form of the Morison equation is applicable only in the case that the frequency of the motion of a structure is the same as that of incident waves. Further investigation is needed to determine the appropriate values of $C_m$ and $C_d$ in the relative velocity form model in waves.

Different forms of $DU/Dt$ can be considered for the fluid inertia term in Equation 2.6. For a body moving in an accelerating flow, $DU/Dt$ in Equation 2.4 can be evaluated by several ways. In the case that the horizontal displacement $x$ of a cylinder is small compared to the wave length, the local form of fluid particle acceleration $DU/Dt = \partial U/\partial t$ can be used. In this case the relative form of the Morison equation will be nonlinear only in the drag force.

Newman [18] has shown that for an accelerating flow and flexible structure, the total fluid particle acceleration is given by $DU/Dt = \partial U/\partial t + (U - \dot{x})\partial U/\partial x$, which includes both local and convective acceleration terms and is the most accurate form for the fluid particle acceleration. In the case of $\dot{x} << U$, the total fluid acceleration expression becomes $DU/Dt = \partial U/\partial t + U\partial U/\partial x$, where again both local and convective terms are present. In these two cases, the relative velocity formulation of the Morison equation is nonlinear in both the drag force and the

fluid inertia force.

As discussed above, the values of the drag and inertia coefficients appropriate to each case need to be used as the Morison equation is empirical. For a cylinder moving in waves, because of the lack of reliable data the two coefficients, drag and inertia coefficients, are usually considered to be equal to those of a fixed cylinder in waves or a surging cylinder in still water. This method is often used, but its suitability is not fully confirmed as previously discussed. So far research concerning the validity of the relative form of the Morison equation has not been made to compare the effects of various forms of the total fluid particle acceleration.

## 2.3 Review of Nonlinear Dynamics of Offshore Structures

Previous studies concerning the nonlinear dynamic behaviour of various types of offshore structures have focused on obtaining a good approximation of dynamic wave loading as well as the harmonic response of the structure, and developing the various techniques to simplify the nonlinearities arising in these systems. To do this various linearization techniques have been used by many researchers, for example, Spanos et al. [19], McNamara et al. [20], and Chakrabati et al. [21]. A comparison of various linearization methods and a perturbation method to deal with the nonlinear drag force is given by Lipsett [22]. It is well known that the solution of a linearized system, though very useful in some cases, can not predict all the nonlinear phenomena which can occur in real systems. Consequently the simplification of environmental conditions by linearization may only give partial results and can not determine the actual system behaviour which governs the system instability and sensitivity to the initial conditions. Because of this reason there is increasing interest in nonlinear behaviour and stability analysis of nonlinear systems. Complex responses have been observed in various models of offshore systems. For most models of compliant offshore systems some assumptions and simplifications are

necessarily made. These include the use of the deterministic forcing which models a regular sea state. Also the inertia and drag coefficients are usually taken as constants determined by typical Reynolds and Keulegan-Carpenter numbers from fixed cylinder experimental tests. Finally, only a single degree of freedom model of the structure is considered in general.

Nonlinear systems of the Duffing type with parametric and external excitation have been studied by Yagasaki [23], Yagasaki et al. [24], and HaQuang et al. [25]. Their results obtained by both analytical and numerical methods have shown that the dynamics of such systems is extremely complex and various nonlinear responses including period doubling and chaotic motion have been observed. It was also shown from the work by HaQuang et al. [25] that such systems can exhibit nonlinear characteristics in their response even at very small amplitudes of the excitation and show enlarged regions of instabilities and chaotic motions compared to the systems with external excitation only.

Bishop and Virgin [9] have described a combined numerical and geometrical approach to study the dynamic behaviour of a moored semi-submersible. The wave exciting force includes a constant drift component. The period doubling route to chaos has been identified. Gottlieb [10] has studied the wave-structure interaction of a multi-point mooring system and performed the stability analysis of this system. The method of harmonic balance and Hill's variational equations have also been employed in his stability analysis. In the model used by Thompson et al. [11], an articulated tower is modeled by a bilinear system which includes a geometrical discontinuity in restoring stiffness. This results in a significant nonlinearity for this system. Thompson et al. [11] have shown that for this simple system the response to the harmonic force can be very complex; various subharmonic responses and chaotic response as well as coexistence of the multiple solutions have been predicted. By introducing additional nonlinearities in restoring force to the bilinear oscillators, another mathematical model for the articulated tower system has been studied by

Choi and Lou [26]. In this model, the nonlinear drag force term is linearized and the wave exciting term proportional to the quadratic fluid velocity in the drag force is neglected. The discontinuity in the nonlinear restoring moment is approximated by a nonlinear continuous function. This is the only nonlinearity in this model and the resulting equation is a Duffing type oscillator. They have observed that as the amplitude of excitation increases, higher-order subharmonic responses and chaotic motion will appear. In addition, jump phenomena, coexistence of multiple solutions and higher-order subharmonics occur as the damping decreases. Also the method of harmonic balance and the Hill's variational equations have been employed to obtain the analytical solutions and the stability criteria for this system. A good agreement has been found between the analytical results and direct numerical integration results. The values of wave height used by Choi and Lou were: $H = 7.62m$ to $45.72m$.

In the model of the articulated tower used by Gottlieb et al. [27], the exact forms of the restoring and hydrodynamic exciting moment were retained. Since the tower displacement was assumed small, the only nonlinearity in this model is the nonlinear drag force. Liaw [28] has also studied a model similar to the one used by Gottlieb et al. [27] except that the convective terms in fluid particle acceleration expression were included in Liaw's model. Therefore Liaw's model includes the nonlinear drag force and the nonlinear exciting force arising from the convective terms in the fluid acceleration. Both models consider the unconstrained articulated tower and complex responses have been observed in both models. The work by Fujino and Sagara [29] has also indicated the existence of the complex response of the articulated tower. The nonlinearities in their model include a nonlinear restoring force and a nonlinear fluid damping which is then expressed by finite terms of Fourier series in their stability analysis.

While numerical time domain simulation has been the primary tool for the solutions of offshore nonlinear systems, analytical methods such as harmonic balance

method and modified multiple scales perturbation method have also been applied to some systems. Due to the nonlinear quadratic drag force, some approximation is usually made when applying these methods to offshore structure systems. The harmonic balance method complemented by local stability analysis was applied to a moored single-point system modeled by cubic polynomials by Choi and Lou [26] and higher order polynomials by Fujino and Sagara [29]. The drag term in the study by Fujino and Sagara [29] was approximated by expressing the structure velocity dependent term as a linear combination of harmonic functions and the fluid velocity was neglected. Other examples of using harmonic balance method to perform local stability analysis are the articulated system and multi-point mooring system used by Gottlieb [10] and Gottlieb et al. [27]. The multiple scales perturbation was used to analyze a ship roll model by Nayfeh et al. [30, 31]. This model includes two nonlinearities, nonlinear restoring force approximated by a polynomial including a cubic and a higher order functions, and nonlinear cubic damping term.

The effort has also been made to determine which nonlinearity has a dominant influence on the occurrence of the complex behaviour of compliant offshore structures. So far two nonlinearities arising in equations of motion of offshore mooring systems have been studied extensively: (a) geometrical nonlinearity and structural discontinuity in the cable or mooring restoring force; (b) the nonlinear drag force. In order to analyze the nonlinear restoring force, the nonlinear drag force is usually simplified by using various linearization techniques. The studies by Thompson et al. [11], Choi and Lou [26], Bishop and Virgin [9] have indicated that the geometrical nonlinearity and structural discontinuity in restoring force can induce subharmonic and chaotic responses for certain values of system parameters. The model used by Gottlieb [10] of a multi-point mooring system incorporates the nonlinear restoring force, nonlinear quadratic drag force, and the nonlinear convective inertia force.

Liaw [32] has compared the solutions obtained from several models of articulated tower with various approximations to the wave kinematics and nonlinear drag force.

One of conclusions that Liaw claimed is that the complex response will likely occur only if the wave properties are evaluated at the deformed positions of the structure, which means the wave exciting force includes the convective component. However, complex responses were also observed when the wave properties are evaluated at the undeformed position of the articulated tower in the model used by Gottlieb et al. [27]. Note that the tower angular displacement was assumed to be small in this model so that the nonlinear drag force is the only important nonlinearity in the equation of motion. The conclusion by Gottlieb et al. [27] is apparent: nonlinearity of the drag force has a dominant effect on the occurrence of complex response since this is the only nonlinearity in this model. This seems to be in contrast to the conclusion of Liaw [32]. It is this apparent discrepancy that will be addressed in this thesis.

The existing current research indicates the need for further investigation of the complex dynamic system behaviour of nonlinear systems to provide a comprehensive understanding of behaviour of compliant offshore structures. Although complex behaviour has been observed in different models, the system parameters typical for a real structure are rarely used. Also further research is required to identify the effects of various nonlinearities on the system behaviour.

## 2.4 Useful Tools of Nonlinear Dynamic Analysis

As mentioned before, chaotic response has a very strong dependence on initial conditions. This makes long term prediction of the system response impossible. However, some universal features, qualitative and quantitative, have been found to identify chaotic motion in nonlinear dynamic systems. These features, such as Feigenbaum numbers, amplitude scaling, subharmonic spectra scaling, all discovered by Feigenbaum [33, 34] as well as Liapunov exponents, are universal in the sense that they do not depend on any particular system. One of the routes to chaos, perhaps

the most common route, is the period doubling route. The first three universal features are associated with period doubling phenomenon. The precursor of chaos in this case is the appearance of a sequence of period doubling bifurcations. That is, the periodicity of the system response doubles each time the solution of system changes qualitatively by varying a system parameter. The local bifurcation, the behaviour of the system in the vicinity of a critical point (the bifurcation point), reveals the qualitative change of system response. On the other hand, the global bifurcation indicates the route to chaos. These changes can be qualitatively or quantitatively measured by using the universal features under discussion and other useful tools. The discovery of the universality of chaotic behaviour indicates the order within chaos.

Some useful tools for studying dynamic systems and the methods to quantitatively or qualitatively measure the irregularity of the system response are discussed in the following. These tools will be used to describe the response of an articulated tower with harmonic wave forcing in the remaining part of this thesis.

### 2.4.1 Poincaré Section

A very useful plot to show the properties of dynamic systems is the phase plane diagram in which the velocity is plotted as a function of the displacement. Frequently, this diagram consists of a continuous curve which shows the evolution of the system state in the phase space. Alternatively, if, instead of looking at the motion continuously, we look at it at discrete times, then it is possible to construct this diagram by sampling the phase plane trajectory at specific times, for example, equal to multiples of forcing period and the motion will appear as a sequence of dots on the phase plane.

The diagram for the sampled phase plane is called a Poincaré section as the continuous phase trajectory is "cut" periodically. These sampled points will make

sense only if the system motion reaches the steady state, in other words, sampling is done after the transient has died out. Although some information is lost in doing so this technique is found very useful especially for complicated phase plane trajectories. These sampled points, fixed in each forcing cycle, are strictly comparable (see for example, Thompson [8]) since the magnitude and the phase of the periodic forcing function are identical at these points.

The Poincaré section simplifies the phase plots but still retains the main features of the dynamical system. In general, the sampling period is usually taken as that of the excitation. Then the number of the points on the Poincaré section tells the order of solution. A finite number of points on the Poincaré section represent a periodic response since the response will repeat after some time. For example, for periodic response with same period as that of forcing, usually called harmonic response or period one solution, only one point will be shown on the Poincaré section as motion repeats after every forcing period; for a periodic response with a period twice that of forcing, called a period two response, there are two distinct points on the Poincaré section, indicating that motion bounces between these two points and repeating occurs after every two forcing periods. Similarly, for a period $n$ solution, motion repeats after every $n$ forcing periods and there are $n$ different points on the Poincaré section. For chaotic motion, in which the repeating period is infinity, the Poincaré section will contain infinite numbers of points which do not repeat. The high organization of these points, often called the strange attractor showing the stretching, folding and contracting in phase space, is a defining characteristic of chaotic motion.

### 2.4.2 Liapunov Exponents

Liapunov exponents provide a way to test the sensitivity of the system to changes in initial conditions. For every dynamical system, there is a spectrum of Liapunov

exponents that tells how lengths, areas and volumes change in the phase space. Liapunov exponents, which have proven to be the most useful dynamical test for chaotic systems (see for example, Moon [5]), are the average exponential rates of divergence or convergence of nearby orbits in the phase space. Since nearby orbits correspond to almost identical initial states, exponential orbital divergence means that systems will soon behave quite differently, implying the loss of the information or predictive ability. Any system containing at least one positive Liapunov exponent is often defined as being chaotic (see for example, Moon [5]).

In general, for an n-dimensional system, the time evolution of n principal axes with unit length is monitored and what Liapunov exponents measure is changes in length in the direction of these principal axes after some time. If $d_{0i}(t_{k-1})$ is the initial difference between two nearby points at time $t_{k-1}$ and evolves to $d_i(t_k)$ at a later time $t_k$, the $i^{th}$ Liapunov exponent, $\lambda_i$, is defined as (see for example, Moon [5])

$$\lambda_i = \frac{1}{t_N - t_0} \sum_{k=1}^{N} \ln \frac{d_i(t_k)}{d_{0i}(t_{k-1})}, \tag{2.7}$$

where $t_0$ and $t_N$ are initial and final time, $N$ is the number of time increments.

For continuous time-dependent dynamical systems without a fixed point Haken [35] has shown that at least one Liapunov exponent is identically zero, corresponding to the slowly changing magnitude of a principal axis. Axes that are on average expanding or contracting correspond to positive or negative exponents respectively. A consequence is that for a dissipative system at least one Liapunov exponent must be negative, ensuring that the sum of all the Liapunov exponents is negative because of the dissipation. The signs of the Liapunov exponents provide a quantitative measure of the dynamics of a system. In a one-dimensional discrete system, there is only one Liapunov exponent which is positive for chaos, zero for a marginally stable orbit, and negative for a periodic orbit. The well known logistic equation (see for example, Moon [5]) is an example of a one dimensional discrete system. A second

order continuous dissipative system (three dimensional system) has three Liapunov exponents. If the system does not have a fixed point, then one Liapunov exponent is zero and one must be negative. The remaining Liapunov exponent can either be zero, positive, or negative. As discussed by Wolf et al. [36], a chaotic system with a strange attractor has the following set of Liapunov exponents $(+, 0, -)$, while the so called two-torus has the set $(0, 0, -)$, and a limit cycle has the set $(0, -, -)$. Note that if the system has an attractive fixed point all Liapunov exponents are negative corresponding to the set $(-, -, -)$.

Various algorithms for calculating the Liapunov exponents are available. Two algorithms, one for data generated by a known set of differential or difference equations, and the other for experimental time series data, of calculating all of the Liapunov exponents have been discussed and studied extensively by Wolf et al. [36]. For second order continuous, dissipative differential systems, at least one of the Liapunov exponents is negative, and one is zero if the system does not have a fixed point so that the largest nonzero Liapunov exponent can be used to determine whether a system response is chaotic or not. One method to calculate the largest nonzero Liapunov exponent is by using the variational equations. Appendix B gives the algorithm of this method. Also see references [5, 36] for details about this method.

### 2.4.3 Fourier Spectrum

One of the characteristics of chaotic motion is the appearance of a broad band spectrum of frequencies in the response even though the system input is a single frequency harmonic excitation. From the theory of Fourier series, or its extension Fourier Transform, it is well known that for harmonic motion, the frequency spectrum will have a single component at the frequency equal to that of the harmonic motion. For periodic motion, the frequency spectrum consists of a component

with frequency equal to that of periodic motion, along with the subharmonics of this component. A broad band spectrum would mean that the motion is random and consequently chaotic for a deterministic system. Thus a signal indicating the period doubling route to chaos could correspond to the appearance of an increasing number of subharmonics of a fundamental frequency component when varying a system parameter. The Fast Fourier Transform technique (FFT) is an efficient way to compute the Fourier Transform. Details of this algorithm can be found in any book on signal processing or numerical analysis such as reference [37].

# Chapter 3

# Formulation of Equations of Motion

The equations of motion of an articulated tower are formulated in this chapter. The relative velocity form of the Morison equation is used to estimate the wave loading on the articulated tower and linear wave kinematics is assumed. The local and different total acceleration expressions are used to evaluate the acceleration of fluid particles. If the local acceleration expression $DU/Dt = \partial U/\partial t$ is used, the only nonlinearity in the equation of motion is the quadratic drag force which depends quadratically on the velocity of fluid particle as well as the velocity of the tower. However, when either form of total acceleration expressions, $DU/Dt = \partial U/\partial t + U\partial U/\partial x$ or $DU/Dt = \partial U/\partial t + (U - \dot{x})\partial U/\partial x$, is used, the resulting equation of motion is characterized by both a nonlinear quadratic drag force and nonlinear wave exciting forces, the latter arising from the convective terms in the total acceleration of the fluid particle. The nonlinear wave exciting forces are a nonlinear function of both the tower displacement and time so that the resulting system is a combined parametric and externally excited system.

## 3.1 Linear Wave Theory

A wave theory which provides the kinematic properties of fluid motion in a wave will be necessary in order to calculate the wave loading acting on structures. There are two main difficulties in developing such a wave theory. The first is that the boundary conditions need to be evaluated at an initially unknown free surface. The second is the fact that the boundary conditions are themselves nonlinear. The nonlinearity in boundary conditions arises from the convective terms in Euler equations appearing as the products of the velocities and their spatial gradients. They can be neglected compared to other terms in the boundary conditions if the wave height is small. Thus a convenient way to obtain the wave kinematics is by assuming small wave height and neglecting convective inertia terms. This is the basic assumption of linear wave theory and the resulting wave properties obtained from it are linear with respect to the wave height, hence the name linear wave theory. Other names for linear wave theory are small amplitude wave theory, sinusoidal wave theory or Airy theory. Also it is required in linear wave theory that the fluid have uniform density and water depth be constant, fluid viscosity and surface tension be negligible, and the wave motion be irrotational.

For a wave with wave height, $H$, water depth, $d$, and wave number, $k$, the velocity components of the water particle given by linear wave theory (see for example, Sarpkaya and Isaacson [12]) are

$$u = \frac{\pi H}{T}\frac{\cosh(kz)}{\sinh(kd)}\cos(kx - \omega_f t); \tag{3.1}$$

$$v = \frac{\pi H}{T}\frac{\sinh(kz)}{\sinh(kd)}\sin(kx - \omega_f t). \tag{3.2}$$

Here $u$ and $v$ are the horizontal and vertical velocity components of water particle respectively, $z$ and $x$ are the vertical and horizontal coordinates respectively with origin at seabed, $T$ and $\omega_f$ are the wave period and frequency, where $\omega_f = 2\pi/T$, and $t$ is time.

For deep water, $kd > \pi$, so that $\sinh(kd) \approx e^{kd}/2$, $\cosh(kd) \approx e^{kd}/2$ and $\tanh(kd) \approx 1$, with the result that the above two equations become

$$u = \frac{\pi H}{T} e^{k(z-d)} \cos(kx - \omega_f t); \tag{3.3}$$

$$v = \frac{\pi H}{T} e^{k(z-d)} \sin(kx - \omega_f t). \tag{3.4}$$

Note that in above equations the components of fluid velocity are a nonlinear function of the horizontal displacement $x$.

The relationship between wave number $k$ and wave frequency $\omega_f$ is obtained from the linear dispersion relation

$$\omega_f^2 = gk \tanh(kd), \tag{3.5}$$

which for deep water is simply

$$\omega_f^2 = gk, \tag{3.6}$$

where $g$ is the gravitational acceleration, and wave number $k$ is given by $k = 2\pi/L$, where $L$ is wave length.

In this thesis linear wave theory will be used to obtain the wave properties.

## 3.2 Morison Equation

An empirical equation due to Morison et al. [6] has been widely used in both research and offshore engineering to obtain the wave loading for slender structures since it was first proposed in 1950. The Morison equation is based on the assumptions that the presence of the structure does not affect the wave field and the wave forces on a fixed structure can be expressed as the sum of a drag force which is quadratic in the fluid velocity and an inertia force which is linear in the fluid acceleration. There are several parameters which affect the validity of the Morison equation. The first parameter is the diffraction parameter $D/L$, the ratio of the

diameter of structure to the wave length. For slender structures where $D/L < 0.2$, the lateral dimension of structure is small enough in relation to the wave length so that the incident wave characteristics remain unchanged. In this case diffraction effects become unimportant and the Morison equation can be applied to estimate the force due to wave action. The second parameter is the Keulegan-Carpenter number $K_c$, which is proportional to the ratio of amplitude of water particle motion to the structure diameter and is defined as

$$K_c = \frac{U_m T}{D} = 2\pi \frac{A}{D} \tag{3.7}$$

where $U_m$ is the velocity amplitude of the flow, and A is the amplitude of water particle motion. The importance of $K_c$ is based on the fact that the drag forces on the structure in an oscillatory wave flow are dominated by the separation of flow behind the structure and the formation of large vortices. For small values of $K_c$, the flow does not separate from the structure. In this case, drag forces are very small, inertia forces dominates and the potential flow diffraction theory will be necessary to predict the wave forces. For large values of $K_c$, on the other hand, the wave flow separates from the structure eventually resulting in the development of vortices. Drag forces will then be large and the Morison equation is appropriate for calculating the wave forces acting on the structure.

As previously discussed in section 2.2, for a flexible cylinder with diameter of $D$ subjected to regular wave excitation, the relative velocity formulation of the Morison equation gives the wave loading per unit length as

$$F = \rho \frac{\pi D^2}{4} C_m \frac{DU}{Dt} - \rho \frac{\pi D^2}{4} (C_m - 1)\, \ddot{x} + \frac{1}{2} \rho D C_d \, |U - \dot{x}| \, (U - \dot{x}), \tag{3.8}$$

where $\rho$ is the fluid density, $C_m$ and $C_d$ are the inertia and drag coefficients, $U$ and $DU/Dt$ are the velocity and total acceleration of the fluid particle respectively. The dependence of the coefficients $C_m$ and $C_d$ as a function of the Reynolds number, Keulegan-Carpenter number have been measured by many researchers for fixed cylinders as summarized by Sarpkaya and Isaacson [12].

It is common to assume that these fixed cylinder coefficients also apply to the flexible cylinder case for the appropriate Reynolds number and Keulegan-Carpenter number.

## 3.3 Equations of Motion of Articulated Offshore Tower

The articulated tower considered in this thesis is modeled as a uniform rigid body with circular cross section shown in Figure 3.1. The tower is pinned at sea floor, standing vertically under its own buoyancy. Mathematically, it is essentially an inverted pendulum with the pitch angle $\theta$ being the only degree of freedom. As shown in Figure 3.1, $F_B$ is the buoyancy force of the tower acting at point $B$, the buoyancy center, which is located at a distance $L_B$ from the tower base, $W$ is the total tower weight, $G$ and $L_W$ are the mass centre of the tower and the distance from the tower base to $G$.

The equation of motion of the articulated tower can be written as

$$I\ddot{\theta} + C\dot{\theta} + R(\theta) = M(\theta, \dot{\theta}, t) \tag{3.9}$$

where $\dot{}$ denotes the differentiation with respect to time, $I$ is the moment of inertia of the tower about its base, $C$ is the structural damping coefficient including the friction at joint $O$, $R(\theta) = (F_B L_B - W L_W)\sin\theta$ and $M(\theta, \dot{\theta}, t)$ are the restoring moment and the moment of total fluid forces about the base of the tower respectively.

It is assumed in this thesis that the tower angular displacement, $\theta$, is small so that the presence of the tower does not affect the wave field and that the total fluid force acting on an infinitesimal structural element $dl$, located at a distance $l$ from the tower base, can be obtained from the relative velocity formulation of the Morison equation(equation 3.8). Thus the restoring moment, $M(\theta, \dot{\theta}, t)$, can be obtained by integrating the fluid force along the tower, that is

$$M(\theta, \dot{\theta}, t) = \int_0^d F\, l\, dl \tag{3.10}$$

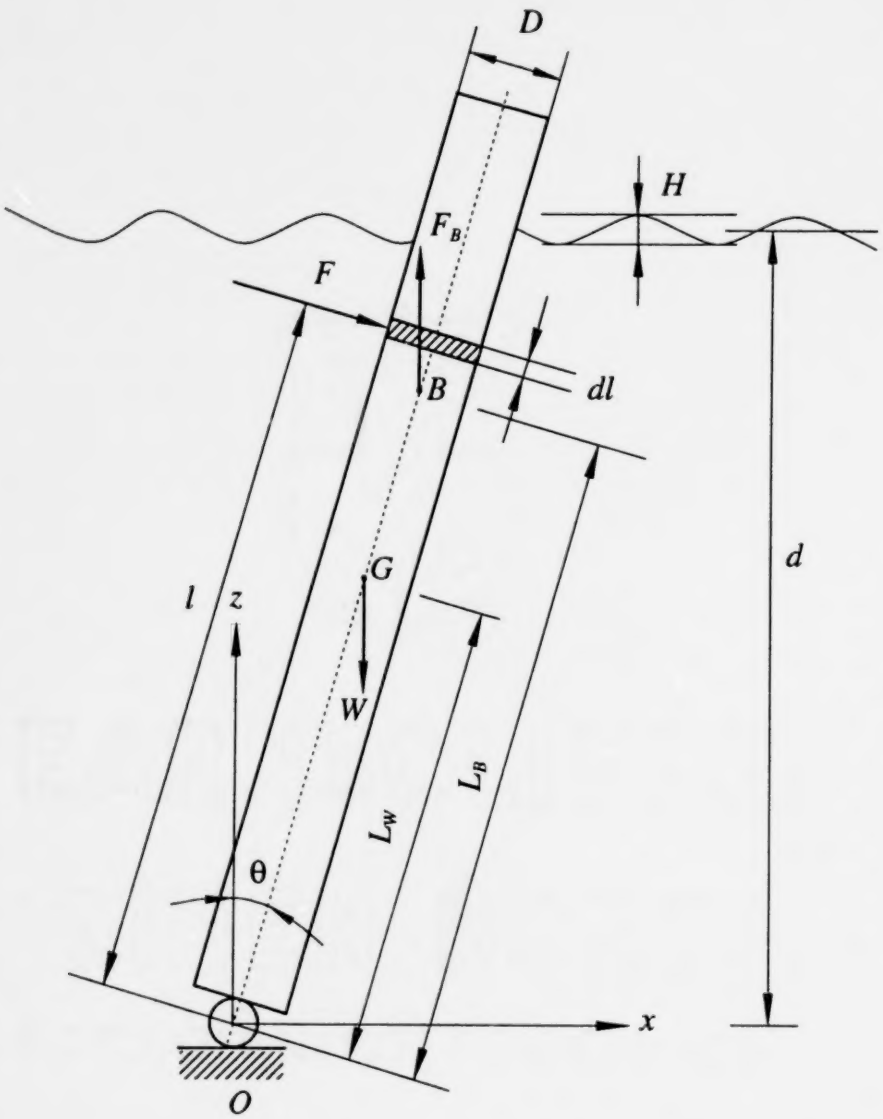


**Figure 3.1:** Model of the articulated tower system

with $F$ being given by Equation 3.8. Substitution of $F$ and $x \approx l\ \theta$, $z \approx l$ into Equation 3.10 gives

$$\begin{aligned} M(\theta, \dot{\theta}, t) &= \rho \frac{\pi D^2}{4} C_m \int_0^d \frac{DU}{Dt}\, l\, dl - \rho \frac{\pi D^2}{4} (C_m - 1)\, \ddot{\theta} \int_0^d l^2\, dl \\ &\quad + \frac{1}{2}\, \rho D C_d \int_0^d \left| U - l\, \dot{\theta} \right| (U - l\, \dot{\theta})\, l\, dl. \end{aligned} \tag{3.11}$$

The velocity of fluid particle in the direction of the tower motion, $U$, is given by linear wave theory as

$$U = u \cos\theta + v \sin\theta \tag{3.12}$$

which for small $\theta$ becomes

$$U \approx u. \tag{3.13}$$

There are several ways that can be used to evaluate the fluid particle acceleration $DU/Dt$ in above equation. It can be given by the local acceleration expression

$$\frac{DU}{Dt} = \frac{\partial U}{\partial t}, \tag{3.14}$$

which can be justified only if the convective terms in the total acceleration expression are small compared to local acceleration. When convective terms are not small, therefore can not be neglected, the total acceleration expressions of either form

$$\frac{DU}{Dt} = \frac{\partial U}{\partial t} + U \frac{\partial U}{\partial x} \tag{3.15}$$

or

$$\frac{DU}{Dt} = \frac{\partial U}{\partial t} + (U - \dot{x}) \frac{\partial U}{\partial x}, \tag{3.16}$$

can be used to evaluate the fluid acceleration. Here $\dot{x}$ is equivalent to $l\dot{\theta}$.

As mentioned earlier in Chapter 2, the most accurate form for the fluid particle acceleration, Equation 3.16, was derived by Newman [18]. Note that both local

and convective terms are included in this equation. However, if the assumption of $\dot{x} << U$ can be satisfied, a simpler expression for fluid particle acceleration can be obtained by neglecting the term involving $\dot{x}$, which results in Equation 3.15. This expression, which again includes both local and convective terms, has been used by some researchers, for example, Liaw [32]. Finally, if the horizontal displacement $x$ of the structure is small compared to the wave length $L$, a linearized expression, which simply includes the local acceleration term and is the simplest form for the fluid particle acceleration, can be given by Equation 3.14.

As will be seen later in numerical simulations, neglecting the convective terms in either Equation 3.15 or 3.16 will mean neglecting all interesting nonlinear responses in the system response. Also it will be shown that the response of the articulated tower using either form of the total acceleration expressions will exhibit complex responses including subharmonic and chaotic responses, as well as jump phenomenon and coexistence of multiple competing solutions. This consequently implies the important role of the convective terms in resulting complex responses.

It should be noted that the fluid particle acceleration given by Equation 3.14 is a function of time and distance $l$ only as it is evaluated at the undeformed equilibrium position. This is true when the wave height is small and the horizontal displacement $x$, here, $x \approx l\,\theta$, of the tower is negligible compared to the wave length $L$. However, the fluid particle acceleration given by either Equation 3.15 or Equation 3.16, on the other hand, is a function of time, distance $l$ as well as the horizontal displacement $x$ of the tower. Sarpkaya and Isaacson [12] have given a comparison of the local and total horizontal accelerations for different wave heights, showing the larger difference between these two for increasing wave height. Isaacson [38] has also studied the theoretical influence of convective acceleration terms on the inertia force for fixed body problems, showing that the effective inertia coefficient is generally less than or equal to the true inertia coefficient so that the inertia forces calculated in the conventional manner will generally overestimate the actual inertia force.

Using the local acceleration to estimate the fluid particle acceleration leads to the following equation of motion of the articulated tower

$$\ddot{\theta} + \mu\dot{\theta} + \omega_n^2\theta = \lambda K_\lambda \int_0^{kd} (u^* - \frac{s\dot{\theta}}{\omega_f}) \left| u^* - \frac{s\dot{\theta}}{\omega_f} \right| sds - \varepsilon K_\varepsilon(kH)\sin\omega_f t. \quad (3.17)$$

Note that this equation is obtained by dividing Equation 3.9 by $I + I_a$.

If either form of the total acceleration expressions is used, then the equation of motion is of the form of

$$\ddot{\theta} + \mu\dot{\theta} + \omega_n^2\sin\theta = \lambda K_\lambda \int_0^{kd} (u^{**} - \frac{s\dot{\theta}}{\omega_f}) \left| u^{**} - \frac{s\dot{\theta}}{\omega_f} \right| sds + g(\theta,\dot{\theta},t), \quad (3.18)$$

where $g(\theta,\dot{\theta},t)$ is the inertia forces due to the fluid inertia and its form depends on which total acceleration expression is used. If Equation 3.15 is used, then $g(\theta,\dot{\theta},t)$ is given by

$$g(\theta,\dot{\theta},t) = g_1(\theta,\dot{\theta},t); \quad (3.19)$$

alternatively, if Equation 3.16 is used instead, then

$$g(\theta,\dot{\theta},t) = g_1(\theta,\dot{\theta},t) + g_2(\theta,\dot{\theta},t), \quad (3.20)$$

where functions $g_1(\theta,\dot{\theta},t)$ and $g_2(\theta,\dot{\theta},t)$ are given by

$$\begin{aligned} g_1(\theta,\dot{\theta},t) = {} & \varepsilon K'_\varepsilon(kH)\left[\frac{kd(1+\theta^2)-(1-\theta^2)}{(1+\theta^2)^2}\sin(kd\theta-\omega_f t)\right. \\ & \left. + \frac{2\theta - kd\theta(1+\theta^2)}{(1+\theta^2)^2}\cos(kd\theta-\omega_f t)\right] \\ & - \frac{\varepsilon K'_\varepsilon}{16}(kH)^2\left[\frac{2kd(1+\theta^2)-(1-\theta^2)}{(1+\theta^2)^2}\sin 2(kd\theta-\omega_f t)\right. \\ & \left. + \frac{2\theta - 2kd\theta(1+\theta^2)}{(1+\theta^2)^2}\cos 2(kd\theta-\omega_f t)\right]; \end{aligned} \quad (3.21)$$

$$\begin{aligned} g_2(\theta,\dot{\theta},t) = {} & \varepsilon K'_\varepsilon(kH)\frac{\dot{\theta}}{\omega_f}\left[\frac{(kd)^2(1+\theta^2)^2 + 2kd(\theta^4-1) + 2(1-3\theta^2)}{(1+\theta^2)^3}\right. \\ & \sin(kd\theta-\omega_f t) \\ & + \frac{-(kd)^2\theta(1+\theta^2)^2 + 4kd\theta(1+\theta^2) - 2\theta(3-\theta^2)}{(1+\theta^2)^3} \\ & \left. \cos(kd\theta-\omega_f t)\right]. \end{aligned} \quad (3.22)$$

The symbols in Equations 3.17 to Equation 3.22 are defined as below

$$s = k\,l, \tag{3.23}$$

$$u^{*} = \frac{kH}{2}\, e^{(s-kd)} \cos\omega_f t, \tag{3.24}$$

$$\mu = \frac{C}{I + I_a}, \tag{3.25}$$

$$\omega_n^2 = \frac{F_B L_B - W L_W}{I + I_a}, \tag{3.26}$$

$$\beta = \frac{I_a}{I_a + I}, \tag{3.27}$$

$$\lambda = \beta\, \frac{C_d}{C_m - 1}\, \frac{6g}{\pi d}, \tag{3.28}$$

$$K_\lambda = \frac{1}{kD}\frac{1}{(kd)^2}, \tag{3.29}$$

$$\varepsilon = \beta\, \frac{C_m}{C_m - 1}\, \frac{3g}{2d}, \tag{3.30}$$

$$K_\varepsilon = \frac{kd - 1}{(kd)^2}, \tag{3.31}$$

$$I_a = \rho \frac{\pi D^2}{4}\frac{d^3}{3}, \tag{3.32}$$

$$K'_\varepsilon = \frac{1}{(kd)^2}, \tag{3.33}$$

$$u^{**} = \frac{kH}{2}\, e^{(s-kd)} \cos(s\theta - \omega_f t). \tag{3.34}$$

The linear dispersion relation (Equation 3.6) has been used in above equations.

Note that in fluid inertia force functions $g_1(\theta, \dot{\theta}, t)$ and $g_2(\theta, \dot{\theta}, t)$, the angular displacement of the tower $\theta$ appears along with nondimensional factor $kd$ in *sin* and *cos* functions. Note that for very deep water, $d$ is large so that the term $kd$ can also be large. Consequently the term $kd\theta$ can be a significant term even though for small oscillations $\theta$ may be very small. The result is that neglecting $kd\theta$ in expressions of the fluid velocity as well as fluid acceleration is not appropriate in this case. It is for this reason that convective acceleration terms play a crucial role in resulting in complex responses of the articulated tower system.

As can be seen in above equations, the resulting equation of motion using either

form of the total fluid particle acceleration expressions is both a parametric and externally excited system since the amplitude of wave exciting forces and damping coefficient are a nonlinear function of the tower displacement $\theta$ as well as time $t$. Also, the wave exciting force includes the higher order component of wave frequency.

With the assumption of angular displacement of the tower $\theta$ being small the inclusion of the nonlinearity, $\sin\theta$, on the left hand side of Equation 3.18, is not important here. It can be seen from Equation 3.18 there are two significant nonlinearities, namely the nonlinear wave force which is a nonlinear function of the angular displacement $\theta$ of the tower, and the nonlinear quadratic drag force which is a nonlinear function of both wave velocity of fluid particle and angular velocity of the tower in above equations. In order to compare the effect of these two nonlinearities on the complex responses of the tower it is worthwhile to discuss the nonlinear drag force further. Defining this drag term as $F_D$, from Equation 3.17 we have

$$F_D = \lambda K_\lambda \int_0^{kd} [(u^*)^2 - 2u^* \frac{s\dot{\theta}}{\omega_f} + (\frac{s\dot{\theta}}{\omega_f})^2]\ sgn(u^* - \frac{s\dot{\theta}}{\omega_f}) sds \tag{3.35}$$

where $u^*$ and $K_\lambda$ are given by Equations 3.24 and 3.30. As it can be seen in Equation 3.35, the first term in the square brackets [ ] is basically a forcing term while second and third terms are linear and quadratic damping terms. Thus $F_D$ provides forcing as well as the damping to the system. They both increase with the wave height and the drag coefficient and decrease with the diameter of tower since $\lambda$ is proportional to $C_d$ and $K_\lambda$ is inversely proportional to $D$ as given by Equations 3.28 and 3.30.

# Chapter 4

# Response of an Articulated Tower

The solutions of various equations of motion are obtained by numerical integration. Integration of the equation of motion includes evaluating the definite integral in the drag force term. Evaluation of this integral is obtained by using a sequence of subroutines from QUADPACK [39] which uses 21 point Gauss-Kronrod procedure with error control. An Adams predictor-corrector adaptive step size and adaptive order numerical method is employed to obtain the solutions of differential equation. The method uses an Adams-Bashforth procedure as the predictor, and an Adams-Moulton formula as the corrector. Further details about this numerical method are given by [40].

All calculations are performed in double precision. In addition, to check the accuracy of numerical simulation, numerical results obtained from the Adams predictor-corrector numerical method for a number of cases were compared to those obtained from a fourth order Runge-Kutta-Felhberg method with adaptive step size and global error assessment. As a result, the solutions computed from both methods in all cases were the same.

In general, the fourth order Runge-Kutta methods need four evaluations of the differential equation to obtain the solution for each step. When a differential equa-

tion is expensive to evaluate, such as the one for the articulated tower considered here which includes the evaluation of an integral in a finite range in every evaluation of differential equation, the use of a Runge-Kutta method can be computationally expensive. However, the Adams predictor-corrector methods are preferable in this case as they need less evaluations of differential equation. It is for this reason that the Adams predictor-corrector method has been chosen to integrate the equation of motion of the articulated tower in this thesis.

Numerical simulations have been carried out for a hundred and thirty cases of different parameters for the equation of motion using the total fluid particle acceleration expression $DU/Dt = \partial U/\partial t + U\partial U/\partial x$. At least two hundred cases for the equation of motion using the local fluid particle acceleration expression $DU/Dt = \partial U/\partial t$ have also been investigated. Several runs have also performed for the total acceleration form of $DU/Dt = \partial U/\partial t + (U - \dot{x})\partial U/\partial x$ to give a comparison of the effects of different forms of the total fluid particle acceleration on the system response. The stable steady state motions of the system are detected by using the Poincaré section that samples the solution at integer multiples of the forcing period after the transients have died out. Each of these sampled Poincaré points is compared to the previous ones and it is thought that a steady state periodic motion is reached if a Poincaré point repeats a previous one within the desired accuracy of $10^{-6}$. Once the steady state motion is identified, the mean amplitude, denoted by $\theta_o$, which is the average of the amplitude in positive part and the amplitude in negative part over one response period, and the period of solution are recorded. Multiple coexisting solutions, if they exist, are searched for by using different initial conditions. The forcing frequency is varied for each set of system parameters so that the frequency response of system can be obtained.

In this chapter the system parameters with their values and results obtained from numerical simulations will be presented and discussed.

## 4.1 System Parameters

There are nine independent parameters in the equation of motion of the articulated tower. They are: parameter $\mu$, which is proportional to the structural damping coefficient, parameter $\beta$, the inertia and drag coefficients $C_m$ and $C_d$, which arise in the Morison equation, wave height $H$, water depth $d$, natural and forcing frequencies $\omega_n$ and $\omega_f$, and the tower diameter $D$.

In order to obtain some preliminary knowledge for the response of real structures, typical values of system parameters are chosen here. Occasionally a parameter value, not commonly encountered, is used for illustrative purposes. Each parameter with its values which are used in this thesis will be discussed in turn as follows:

- Parameter $\mu$

  Parameter $\mu$ is the ratio of the structural damping coefficient $C$ to the sum of inertia moment of the tower $I$, and equivalent inertia moment of water displaced $I_a$; that is $\mu = C/(I + I_a)$. The structural damping coefficient $C$ accounts for the structural damping including the friction of joint $O$ shown in Figure 3.1. In general, the structural damping is very small compared to that of fluid damping, and $\mu$ is set to 0.001 $1/s$ through out this thesis so that the effect of fluid damping can be studied alone.

- Parameter $\beta$

  Parameter $\beta$, given by $\beta = 1/(1 + I/I_a)$, is a quantity which is a measure of the ratio of the tower weight to the weight of water displaced by the tower. Parameter $\beta$ takes larger values for lighter structures and smaller values for heavier structures. Note that $\beta$ is always less than one. Three values, 0.2, 0.5, and 0.7, of $\beta$ are used here in order to see how this parameter affects the response of the articulated tower.

- Inertia and drag coefficients $C_m$ and $C_d$

  As already mentioned in the Chapter 3, the inertia and drag coefficients $C_m$ and $C_d$ both are a function of the Reynolds number $R_e$, Keulegan Carpenter number $K_c$, as well as the relative surface roughness of structure. In what follows the inertia coefficient $C_m$ will be set to 2.0, as the change of $C_m$ with Reynolds number and Keulegan Carpenter number is relatively constant and close to 2 except for a narrow region of Keulegan Carpenter number (see for example, Sarpkaya and Isaacson [12]). Three values of drag coefficient will be considered; $C_d = 0.2, 0.5, 1.0$. Note that for real structures, drag coefficient $C_d$ typically varies from 0.5 to 2.0. The value 0.2 is not typical for a real offshore structure. It is chosen here so that some basic knowledge is gained about how the system behaves when the drag coefficient is extremely small.

- Wave height $H$

  Wave height $H$ is an important parameter of interest and mainly contributes to the amplitude of wave excitation forces. Large wave height means large exciting force. However, increasing wave height also increases the fluid damping as well (see Equation 3.35 in Chapter 3). In order to see which one of these two has a dominant effect on the response of the tower, changing wave height is very important in studying the response of the tower as it will allow us to see changes in response of the system when wave height is varied. The values of wave height used in this thesis are $H = 5m$, $10m$, and $20m$.

- Water depth $d$

  Water depth $d$ is another parameter important for the wave kinematics. Since the effect of a wave with same wave height on the structures in different water depth is different, it is also important to study the response of the system to different water depths. Here the water depth is set to either $d = 100m$ or

$d = 500m$. Note that the other system parameters are chosen such that, for each of these two values of water depth, the articulated tower system is in the range of deep water for linear wave theory.

- Natural frequency $\omega_n$

  Natural frequency $\omega_n$ is the natural frequency of the articulated tower in water and is given by $\omega_n^2 = (F_B L_B - W L_W)/(I + I_a)$, where $F_B$, $L_B$, $W$, and $L_W$ are defined before. It changes with the submerged length of the structure and this submerged length of the structure changes when tower oscillates in response to the wave excitation. Therefore $\omega_n$ is a function of the tower angular displacement $\theta$. But the pitch angle $\theta$ is assumed to be small in this thesis, as will be seen in the numerical results, so that changes of $\omega_n$ varying with pitch angle $\theta$ will be small and the natural frequency $\omega_n$ can be taken as constant. In this thesis, $\omega_n = 0.6rad/s$ is assumed.

- Forcing frequency $\omega_f$

  Forcing frequency, or wave frequency, is one of the most important parameters in the investigation of nonlinear behaviour of offshore structures. In nature, a large number of periodic wave components with different wave heights, periods, and directions of travel occur at the same time in a given sea area. So the real sea state is a randomly varying sea surface elevation of superposition of all of these wave components. Although the model of the wave kinematics used in this thesis is based on a design wave with a single frequency component, it provides a good mathematical model for the so-called regular sea state when one of the wave frequency components becomes dominant. In order to study how this parameter affects the system response, the forcing frequency is used as a basic parameter which is allowed to vary over a realistic range in numerical simulations for each combination of other system parameters.

The lowest value of forcing frequency that can be used here is restricted by water depth limitation to ensure that water depth is in the range of deep water, that is, $d/L > 0.5$ (see for example, Sarpkaya and Isaacson [12]), where $d$ is the water depth and $L$ is the wave length given by $L = 2\pi/k$, and $k$ is the wave number. The diffraction parameter $D/L$, which is the ratio of the tower diameter to the wave length, puts another limitation on the other end of forcing frequency. Specifically the condition $D/L < 0.2$ needs to be satisfied so that the diffraction effects are not important, as has been discussed in Chapter 3. As will be discussed below structure diameters of $1m$, and $3m$, and $5m$ are used in this thesis. This gives the forcing frequency range from about $0.55rad/s$ to $2.0rad/s$, or the corresponding nondimensional frequency ratio range of $\omega_f/\omega_n$ from 0.917 to 3.33 for water depth $d = 100m$; and the forcing frequency range from about $0.25rad/s$ to $2.0rad/s$, or the ratio of $\omega_f/\omega_n$ from 0.417 to 3.33 for $d = 500m$. Note that it is the ratio of the forcing frequency to the natural frequency that is the important parameter here.

- Tower diameter $D$

  Tower diameter $D$ appears explicitly in drag force term in equations of motion of the tower (Equations 3.17, 3.18). With other parameters being fixed, changing tower diameter only affects the amplitude of this drag term. As can be seen in each of the equations of motion, Equation 3.17, or 3.18, both the drag term and nonlinear forcing terms will depend on the wave height $H$. This implies that increasing wave height will increase the amplitude of both the drag term, which mainly provides large fluid damping, and the nonlinear forcing terms. The magnitude of the drag term can be changed by varying either the drag coefficient or the tower diameter. Since the range of drag coefficient is very limited (from 0.5 to 2.0), changing tower diameter provides a way to significantly change the fluid damping term which is of interest in this

thesis. $D = 1m$, $3m$, $5m$ are used here.

Note that other parameters such as natural frequency $\omega_n$, parameters $\beta$, and $\mu$ will also be changed for real structures when the tower diameter $D$ is changed since it appears explicitly in expressions for these parameters. However, in this thesis these two parameters are treated as independent system parameters.

## 4.2 Comparison of Solutions of Equations

Numerical simulation has been carried out for the equation of motion of an articulated tower using different fluid particle acceleration expressions. In this section the solutions obtained from numerical simulations for these cases will be compared and discussed. In each case, the mean amplitude, $\theta_o$, of the system response over one response cycle is plotted with respect to nondimensional frequency $\omega_f/\omega_n$, the ratio of forcing frequency to natural frequency of structure in water, in all figures of frequency response presented in this chapter. The $n$ in each figure represents the order of the solution and different solutions of different order are plotted with a different symbol.

A response is called harmonic or period one solution, or response of order $n = 1$ if the period of response is as the same as that of the forcing. A response will be called subharmonic response of order $n = 2$ , or period two solution if the period of response is two times that of the forcing. This is also called $1/2$ subharmonic response since the response frequency is half that of the forcing frequency. Similarly, a response with a period equal to three times that of the forcing will be called period three solution, or subharmonic response of order $n = 3$, or $1/3$ subharmonic response, and so on.

First, for the equation of motion using the local fluid particle acceleration, over two hundred cases of different values of system parameters have been investigated numerically. However, nonlinear responses such as subharmonic or chaotic response

have not been found in any of these cases. The frequency response for one of these cases is shown in Figure 4.1(a). The system parameters used for this figure are: $d = 100m$, $H = 10m$, $D = 3m$, $C_m = 2.0$, $C_d = 0.2$, $\omega_n = 0.6rad/s$, and $\beta = 0.7$. In this figure only one resonance, the fundamental resonance at $\omega_f/\omega_n = 1$, is seen and the response period is always the same as the forcing period. Consequently the solutions for the frequency ratio range investigated here in this case are all period one solution, or harmonic solution of order $n = 1$. On the other hand, the solutions shown in Figure 4.1(b), obtained from the equation of motion using the total fluid particle acceleration $DU/Dt = \partial U/\partial t + U\partial U/\partial x$, with same set of parameter values indicate a wide variety of solutions with response periods ranging from one time ($n = 1$) to twelve times ($n = 12$) that of the forcing. Also shown in Figure 4.1 (b) are the subharmonic resonances near $\omega_f/\omega_n = 2$ and 3 respectively, which are not seen in Figure 4.1 (a), in addition to the fundamental resonance. It can be seen from this figure that if the total acceleration is used to evaluate the fluid acceleration, then additional subharmonic responses are predicted, implying that the nonlinear convective term plays an important role on the appearance of subharmonic and chaotic responses. Therefore it is important to include the convective term in the equation of motion for articulated tower system.

Notice that when the local acceleration expression $\partial U/\partial t$ is used to evaluate the fluid acceleration, the drag force is the only nonlinearity in the system. It turns out that for the system parameter range that has been investigated in this thesis the nonlinearity in drag force is not important for complex responses of the articulated tower system. The results shown here are in contrast to those obtained by Gottlieb et al. [27], who studied the same articulated tower problem and claimed that the system can exhibit complex responses when the local fluid acceleration is used.

For reference all the solutions computed for the articulated tower using the local acceleration expression in a large variety of system parameters are listed in Appendix A. As can be seen from these results only $n = 1$ solutions have been found for this

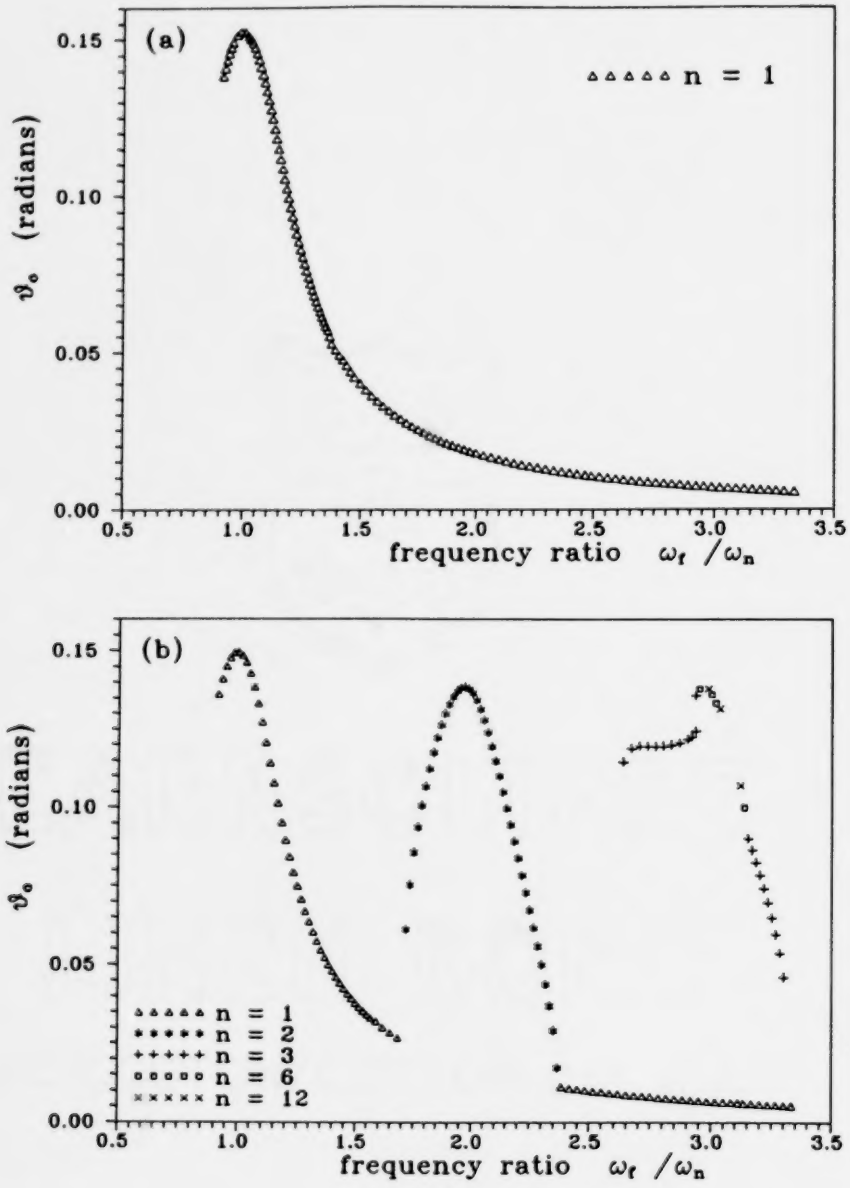


**Figure 4.1:** Frequency response of the tower using local and total acceleration with parameters: $d = 100m$, $H = 10m$, $D = 3m$, $C_m = 2.0$, $C_d = 0.2$, $\omega_n = 0.6rad/s$, $\beta = 0.7$. (a) Using $\partial U/\partial t$; (b) Using $\partial U/\partial t + U\partial U/\partial x$.

wide variety of system parameters.

The importance of the convective term also can be seen from the discussion below. Recall that the fluid velocity in the direction of the tower motion, located at a vertical distance $z$ from the base of the tower, is approximately given by

$$U \approx u = \frac{\pi H}{T} e^{-k(z-d)} \cos(kl\theta - \omega_f t) \tag{4.1}$$

in which $\theta$ appears along with the nondimensional parameter $kd$ and $z$ can be approximated by $l$. In the case of deep water and higher forcing frequencies, such as in subharmonic frequency range, $kd$ is large so that the variation of the fluid velocity with respect to $\theta$ may not be small, although the tower angular displacement $\theta$ is small. It is for this reason that two figures, Figure 4.1(a) and (b), differ greatly from each other in the subharmonic range. Consequently, the convective terms can not be neglected in the expression of fluid acceleration in deep water. The fact that peak value of the fundamental resonance in Figure 4.1(a) and (b) is about the same further supports the above argument that the nonlinear convective term only affects the system response in the higher frequency ratio range.

It is worthwhile to note that in Figure 4.1(b) the peak values of subharmonic resonances are of the same magnitude as that of the fundamental resonance. Also note that in the range of ratio $\omega_f/\omega_n$ from $2.6 \sim 3.3$ period one response coexists with other subharmonic responses with different periods. Note that no coexisting solutions have been found in the range of the second resonance. This indicates that the period one solution becomes unstable in the frequency ratio range associated with the second resonance and becomes stable again in the frequency ratio range after this second resonance. As will be shown in what follows this is a common phenomenon for all frequency response curves with the exception that for some sets of parameters there exists a small instability range for period one solutions in the frequency range near the third resonance.

Figure 4.2 provides a comparison of the system response when two forms of the

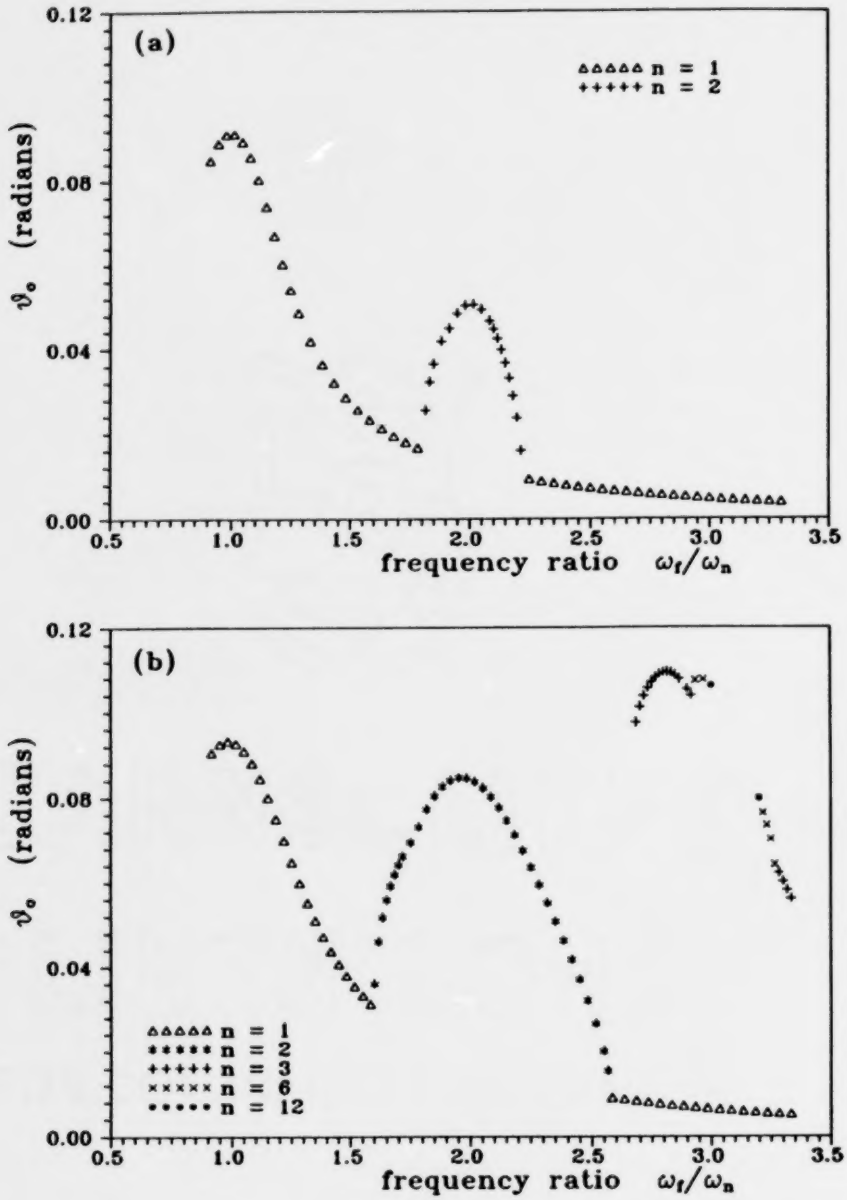


**Figure 4.2:** Comparison of the tower response using total acceleration with parameters: $d = 100m$, $H = 10m$, $D = 5m$, $C_m = 2.0$, $C_d = 1.0$, $\beta = 0.7$, $\omega_n = 0.6rad/s$. (a) Using $\partial U/\partial t + U\partial U/\partial x$; (b) Using $\partial U/\partial t + (U - \dot{x})\partial U/\partial x$.

total acceleration expressions are used. The system parameters used are: $d = 100m$, $H = 10m$, $D = 5m$, $C_m = 2.0$, $C_d = 0.5$, $\beta = 0.7$, and $\omega_n = 0.6rad/s$. It can be seen from this figure that when either form of the total acceleration expression is used, complex responses are predicted. The amplitude of the system response predicted by the equation using $DU/Dt = \partial U/\partial t + (U - \dot{x})\partial U/\partial x$ in general is larger than that predicted using $DU/Dt = \partial U/\partial t + U\partial U/\partial x$. This would mean that subharmonics, chaos, nonlinear phenomena as well as instability problems in the case using the total acceleration form including $\dot{x}$ term may occur even with larger values of the drag coefficient or smaller wave heights than those in the case using the total acceleration form without $\dot{x}$ term in which these phenomena may not appear.

For more comparison between these two see Figures 4.3 and 4.4. It can be seen that there is only small differences between the results of using these two expressions for the fluid particle acceleration. The system parameters used in these two figures are: $d = 100m$, $H = 10m$, $D = 5m$, $C_m = 2.0$, $C_d = 0.5$, $\beta = 0.7$, $\omega_n = 0.6rad/s$; and $d = 100m$, $H = 5m$, $D = 5m$, $C_m = 2.0$, $C_d = 0.5$, $\beta = 0.7$, $\omega_n = 0.6rad/s$ respectively.

Because of the significant difference observed between the prediction of using either local or total acceleration, the remaining results in this chapter are obtained by numerically integrating the equation of motion with the use of the total acceleration expression $\partial U/\partial t + U\partial U/\partial t$. It is felt that results from either form of the total acceleration expressions are a better model of what is really happening for this system.

## 4.3 Frequency Response

A frequency response curve is a very useful plot showing dynamical properties of a system. In this section frequency response curves obtained from numerical

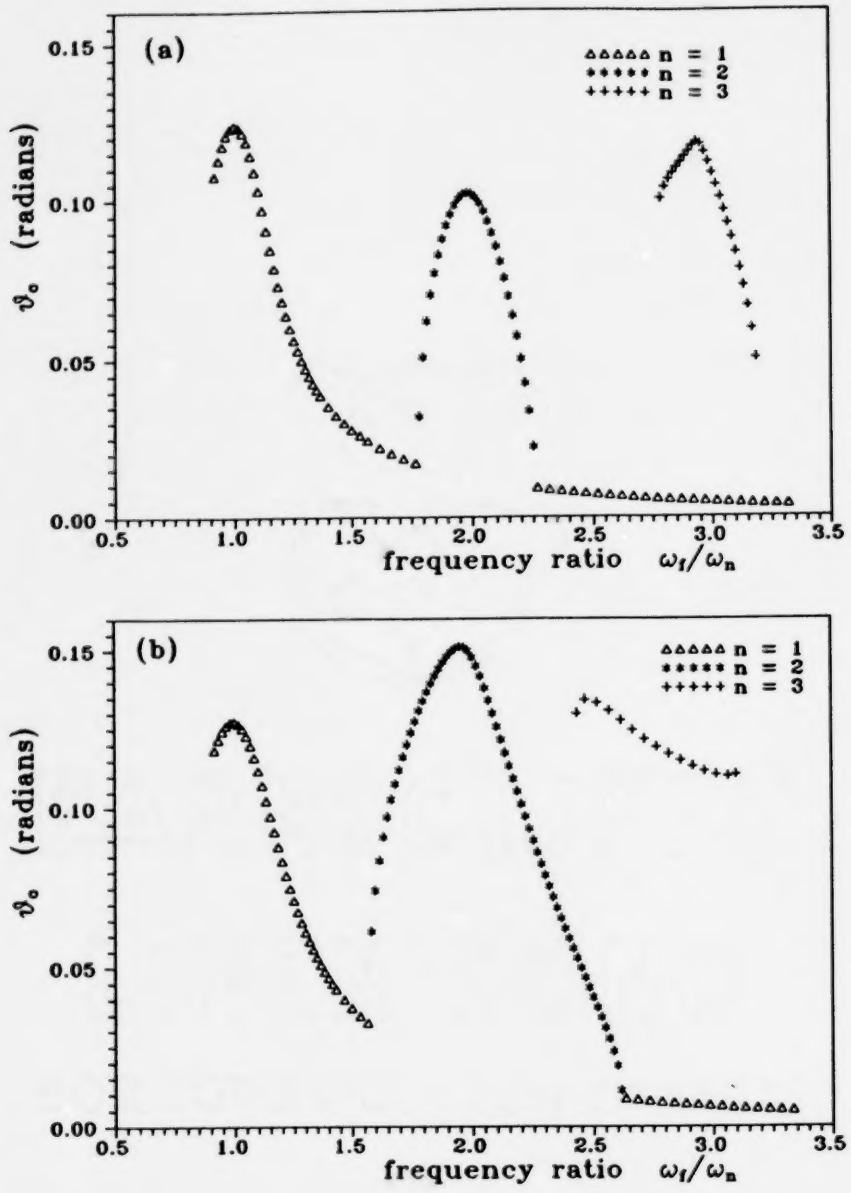


**Figure 4.3:** Comparison of the tower response using total acceleration with parameters: $d = 100m$, $H = 10m$, $D = 5m$, $C_m = 2.0$, $C_d = 0.5$, $\beta = 0.7$, $\omega_n = 0.6rad/s$. (a) Using $\partial U/\partial t + U\partial U/\partial x$; (b) Using $\partial U/\partial t + (U - \dot{x})\partial U/\partial x$.

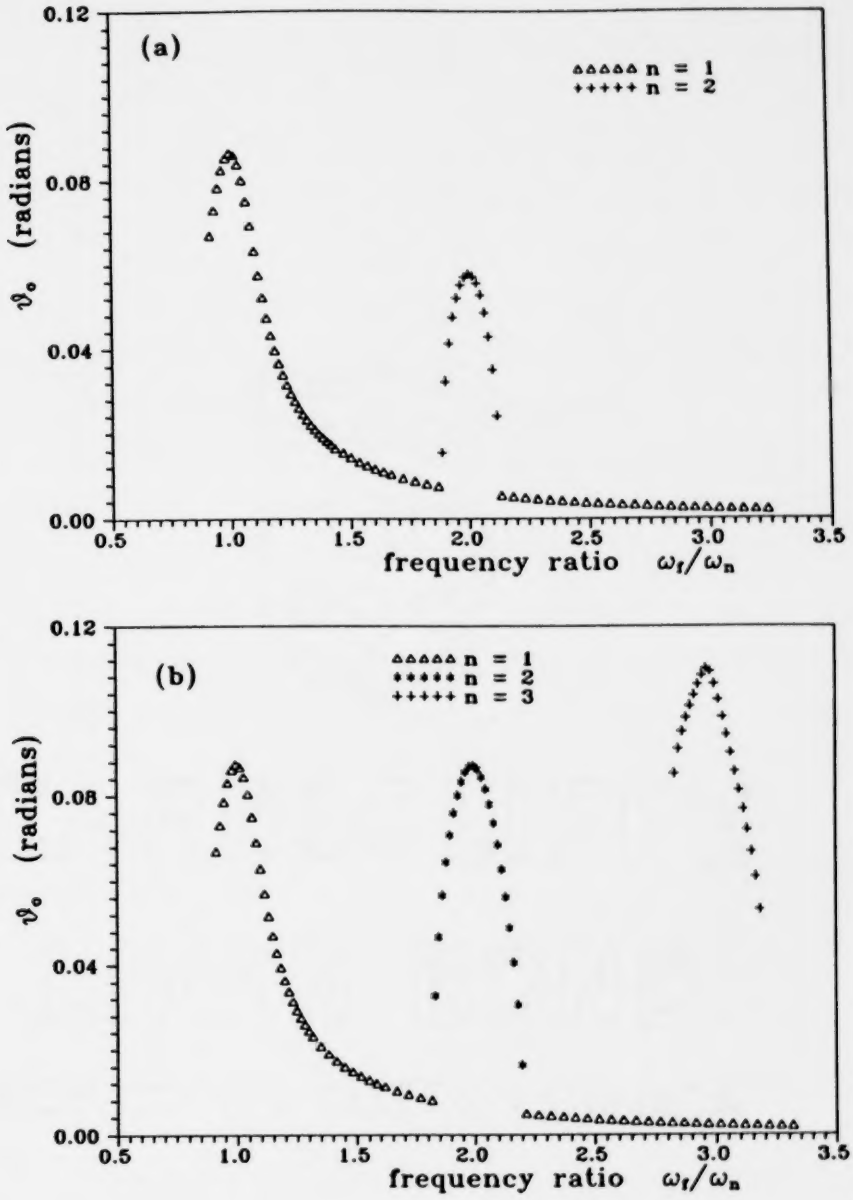


**Figure 4.4:** Comparison of the tower response using total acceleration with parameters: $d = 100m$, $H = 5m$, $D = 5m$, $C_m = 2.0$, $C_d = 0.5$, $\beta = 0.7$, $\omega_n = 0.6rad/s$. (a) Using $\partial U/\partial t + U\partial U/\partial x$; (b) Using $\partial U/\partial t + (U - \dot{x})\partial U/\partial x$.

analysis for some representative parameter values will be discussed.

Figure 4.5 is the frequency response for different values of the drag coefficient, $C_d = 0.2, 0.5, 1.0$. Other system parameters remain unchanged for each of these response curves in this figure and their values are: $d = 100m$, $H = 10m$, $D = 5m$, $C_m = 2.0$, $\omega_n = 0.6rad/s$, and $\beta = 0.7$. For small drag coefficient subharmonic resonances (the second and third resonances) are prominent and are of the almost same magnitude as the fundamental resonance (the first resonance). As drag coefficient increases the peak value of resonances decreases and the width of each resonance gets broader similar to the response of linear systems for increasing damping. Note that all resonances shown here are regular ones in which no jump phenomenon or other stability phenomena occur except the subharmonic resonance associated with period three solutions shown in Figure 4.5(a), where a jump phenomenon is shown near the frequency ratio $\omega_f/\omega_n = 2.75$. There is no change in response period at or after jump and solutions are all period three solutions in the frequency range corresponding to this resonance. Notice the coexistence of period one solutions with period three solutions in Figure 4.5 (a) and (b) in the frequency range associated with the third resonance. It is clearly shown in this figure that the drag coefficient plays an important role on the appearance of subharmonic response. The large fluid damping can significantly reduce the peak value of resonances and damp out all subharmonic resonances if it is large enough. Although other parameters do affect the occurrence of subharmonic and chaotic responses, obviously, the drag coefficient is a very important parameter.

Figure 4.6 shows the system frequency response for different values of the wave height, $H = 5m$, $10m$ and $20m$ respectively. Other system parameter values are: $d = 100m$, $D = 5m$, $C_d = 0.2$, $C_m = 2.0$, $\omega_n = 0.6rad/s$, and $\beta = 0.7$. Since large wave height means large amplitude of the excitation, and consequently large response amplitude, the effect of wave height on the response of the system is obviously important as shown in these figures. As wave height increases, the response

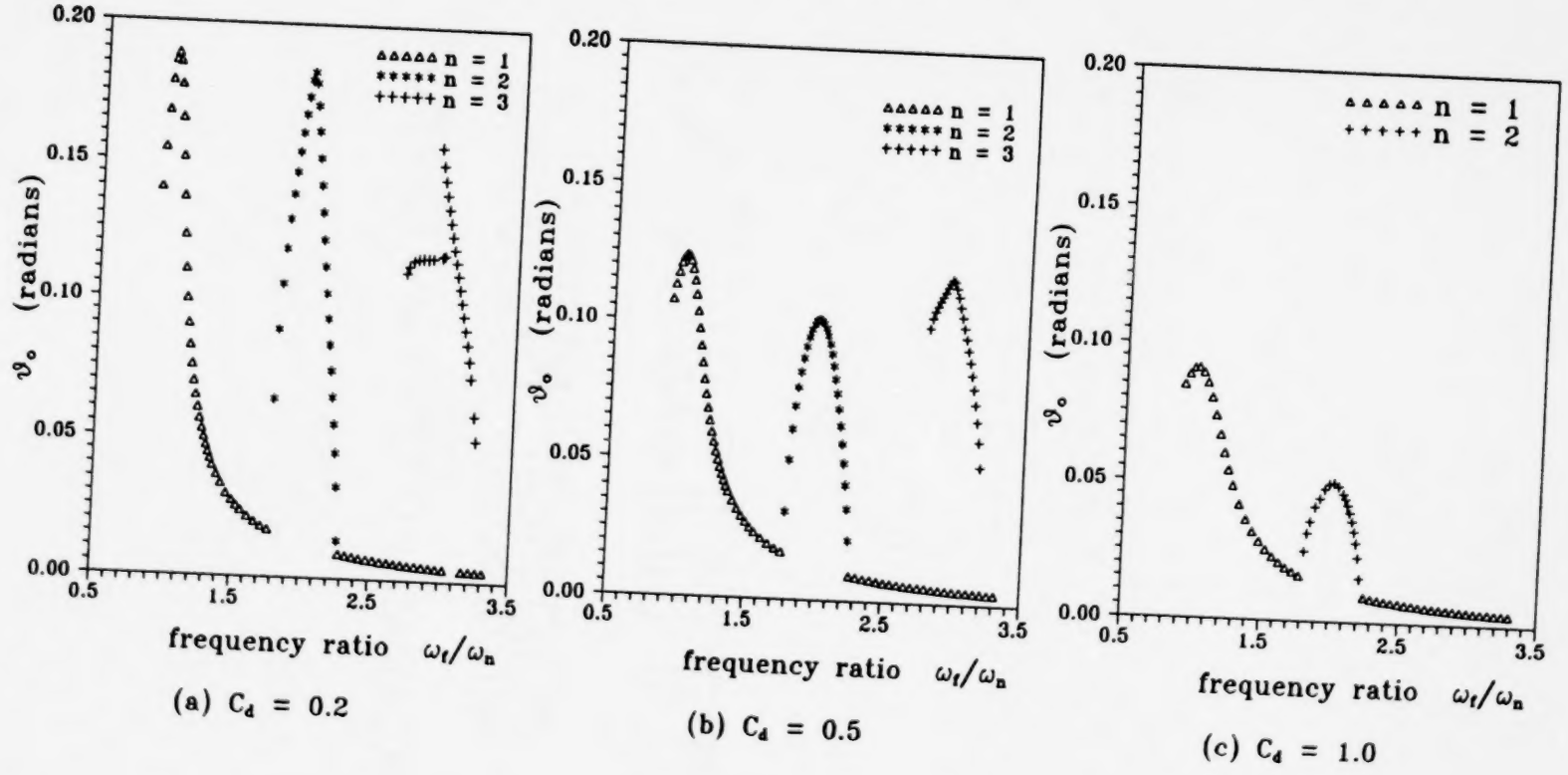


**Figure 4.5:** Frequency response for different values of $C_d$ with parameter: $d = 100m$, $H = 10m$, $D = 5m$, $C_m = 2.0$, $\beta = 0.7$, $\omega_n = 0.6 rad/s$

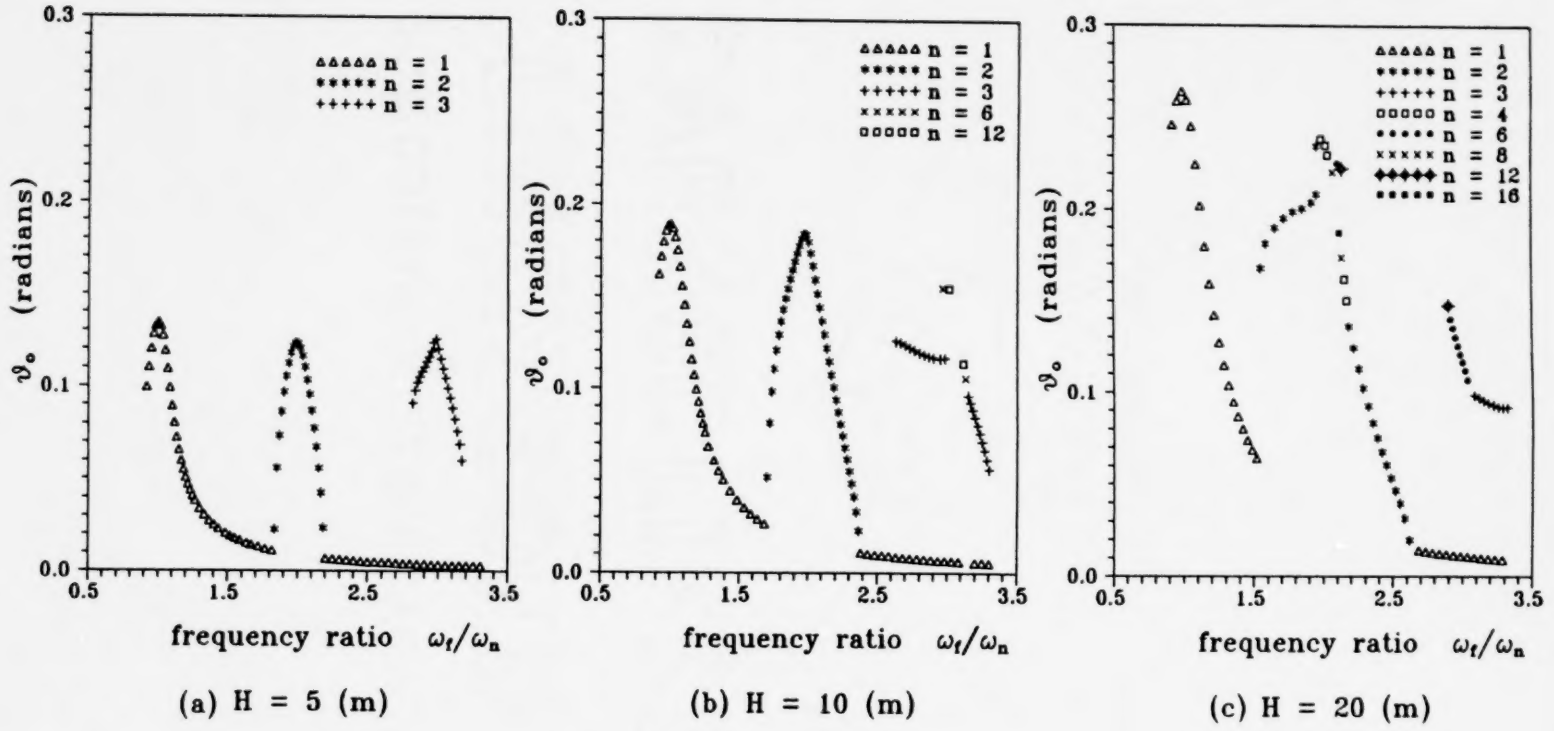


**Figure 4.6:** Frequency response for different values of $H$ with parameter: $d = 100m$, $D = 5m$, $C_m = 2.0$, $C_d = 0.2$, $\beta = 0.7$, $\omega_n = 0.6rad/s$.

amplitude increases; the resonances tend to be more complicated in their shape and stability problems tend to arise. In Figure 4.6(a), all resonances are regular ones, in which no change in response period and no jump phenomenon occur. However, in Figures 4.6(b) and (c) the jump phenomenon and period doubling are seen in some of the resonant peaks. For the third resonance in Figure 4.6 (b), the period three solution with an approximate amplitude of $0.11 radians$ jumps and bifurcates to the period six solution with an amplitude of about $0.16 radians$ and then the solution becomes unstable until an inverse period doubling appears from period twelve to period six, and finally to period three solution. Notice that there is a co-existence of period one solution with other higher order subharmonic solution in the frequency range associated with the third resonance and three different solutions, period one, period three, and period six, coexist at frequency ratio equal to 3.0. In Figure 4.6 (c), the second resonance starts with a sequence of period two solutions, then jumps to another period two solution and bifurcates to a period four subharmonic solution. An infinite period doubling cascade, which may lead to chaotic response, follows after, and finally ends with an inverse subharmonic cascade from period sixteen, to period eight, to period four and to period two solutions. The jump phenomenon happens at frequency ratio close to 1.95 where a pair of different period two solutions coexist. Another branch of subharmonic cascade from period six to period twelve solution appears just beside the period eight solution at frequency ratio about 2.1. The third resonance is only an inverse subharmonic cascade with coexisting period one solutions. Figure 4.6 strongly shows that as wave height increases, the response of the system becomes very interesting, large response and all other nonlinear phenomena can be expected for these system parameters. In the case of small wave height, subharmonic response can also be expected for these system parameters.

Shown in Figure 4.7 is the frequency response of the system for water depths $d = 100m$ and $d = 500m$ with other system parameter values being: $H = 10m$,

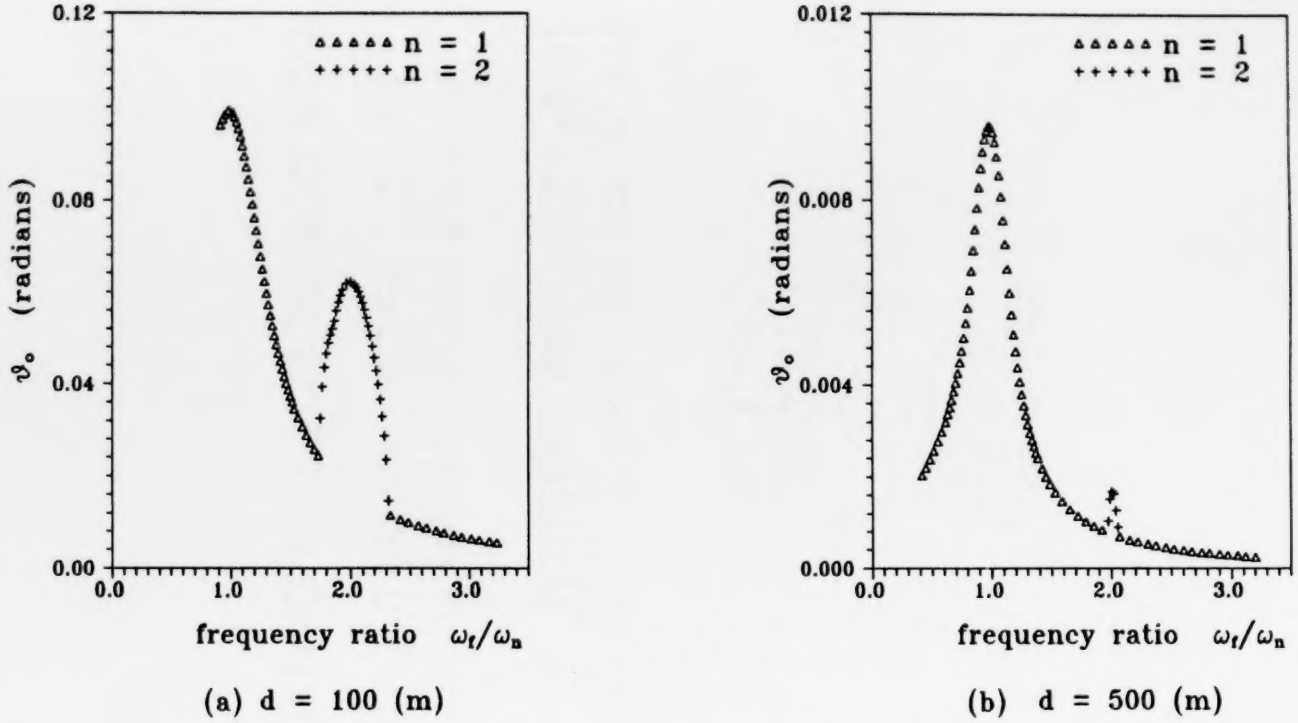


**Figure 4.7:** Frequency response for different values of $d$ with parameter: $H = 10m$, $D = 3m$, $C_m = 2.0$, $C_d = 0.5$, $\beta = 0.7$, $\omega_n = 0.6rad/s$.

$D = 3m$, $C_m = 2.0$, $C_d = 0.5$, $\omega_n = 0.6rad/s$, and $\beta = 0.7$. Note the change of vertical scale between these two figures. When water depth is increased from $100m$ to $500m$ the peak value of the first resonance decreases from about 0.1 *radians* to about 0.01 *radians* and all peak values of the subharmonic resonance become less significant. This indicates that fluid damping increases significantly with the water depth so that subharmonic resonances tend to be less significant in deeper water because of the large fluid damping. The increase of fluid damping with increasing water depth can be seen by carefully studying the quadratic drag force term in either governing equation of the articulated tower. For example, if the integral in quadratic drag term in Equation 3.18 is defined as $I_d$, then

$$I_d = \int_0^{kd} (u^{**} - \frac{s\dot{\theta}}{\omega_f})|u^{**} - \frac{s\dot{\theta}}{\omega_f}| \; s \; ds. \tag{4.2}$$

Recall that $s = 0$ corresponds to the seabed while $s = kd$ corresponds to the still water surface.

From the results of linear wave theory [12] for deep water the moving orbit of fluid particle is approximately circular, and the amplitude of motion decreases exponentially with water depth. For example, the amplitude of fluid particle motion at a depth of half a wavelength below the free surface is only four percent of its value at the still water surface. This means that $u^{**}$, which is related to the velocity of fluid particle, $u$, by $u^{**} = (k/\omega_f)u$, is significant only in a range from the still water surface to a depth equivalent to half a wavelength, that is within the integration limits of $(kd - \pi)$ to $kd$ in above integral. The value of $kd$ can be very large, especially for deep water and the higher forcing frequency range. For example, in the case of $\omega_f = 1.5rad/s$, which corresponds to $k = 0.22961/m$, the value of $kd$ is then given by $kd = 22.96$ for $d = 100m$, and $kd = 114.8$ for $d = 500m$. Outside this range $u^{**}$ is very small and can be neglected so that above integral be written as

$$I_d = \int_{kd-\pi}^{kd} (u^{**} - \frac{s\dot{\theta}}{\omega_f})|u^{**} - \frac{s\dot{\theta}}{\omega_f}| s \; ds - \int_0^{kd-\pi} (\frac{s}{\omega_f})^2 \; \dot{\theta} \; |\dot{\theta}| \; s \; ds. \tag{4.3}$$

The second integral on the right hand side of Equation 4.3 contains a damping term only and does not contribute to the excitation. Hence fluid damping increases significantly when water depth is increased and subharmonics become less prominent and may not appear due to large fluid damping. Note that as water depth becomes very large the model of the articulated tower presented in this thesis, which neglects the deformation of the tower and treats the tower mooring system as a rigid single-degree-of-freedom system, may not be appropriate since the higher modes of deformation of the tower itself could become significant. From this point of view the effect of water depth on the system response needs further investigation.

Figure 4.8 shows the frequency response curves of the system for varying values of parameter $\beta$. The values of $\beta$ used here are: 0.7, 0.5, and 0.2 and other system parameter values are: $d = 100m$, $H = 5m$, $D = 5m$, $C_m = 2.0$, $C_d = 1.0$, and $\omega_n = 0.6rad/s$. This figure shows that variations of $\beta$ do not significantly influence the system response in each case. The fundamental and subharmonic resonances all have almost the same peak value. The only difference between these response curves in this figure is that width of each resonance becomes broader as $\beta$ increases. This is because the fluid damping increases with parameter $\beta$. As already mentioned earlier in this chapter, parameter $\beta$ is a measure ratio of the tower weight to the weight of water displaced by the tower. Since $\beta$ appears explicitly in both nonlinear drag and nonlinear forcing terms, increasing $\beta$ will increase the amplitude of both damping and forcing. These two effects almost cancel out each other resulting in very little difference between frequency response curves of a lighter tower (with larger value of $\beta$) and a heavier tower (with smaller value of $\beta$). However overall results (see Tables 4.1 and 4.3 below) show that a chaotic response is more likely to occur for relatively lighter structures.

The variations of the tower response with tower diameter $D$ are shown in Figure 4.9 with other system parameters being: $d = 100m$, $H = 5m$, $C_m = 2.0$, $C_d = 0.5$, $\beta = 0.5$, and $\omega_n = 0.6rad/s$. As can be expected, the mean response amplitude

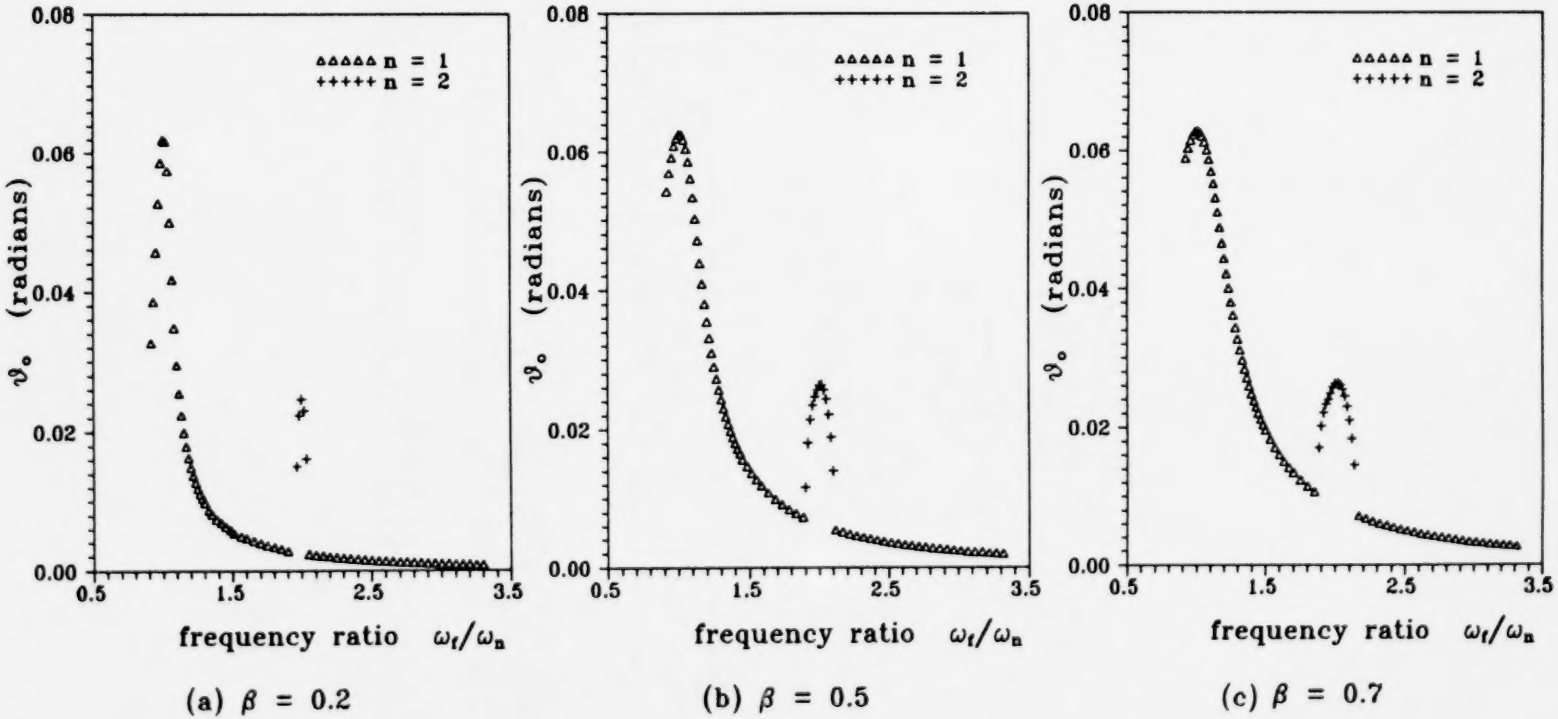


**Figure 4.8:** Frequency response for different values of $\beta$ with parameter: $d = 100m$, $H = 5m$, $D = 5m$, $C_m = 2.0$, $C_d = 1.0$, $\omega_n = 0.6rad/s$.

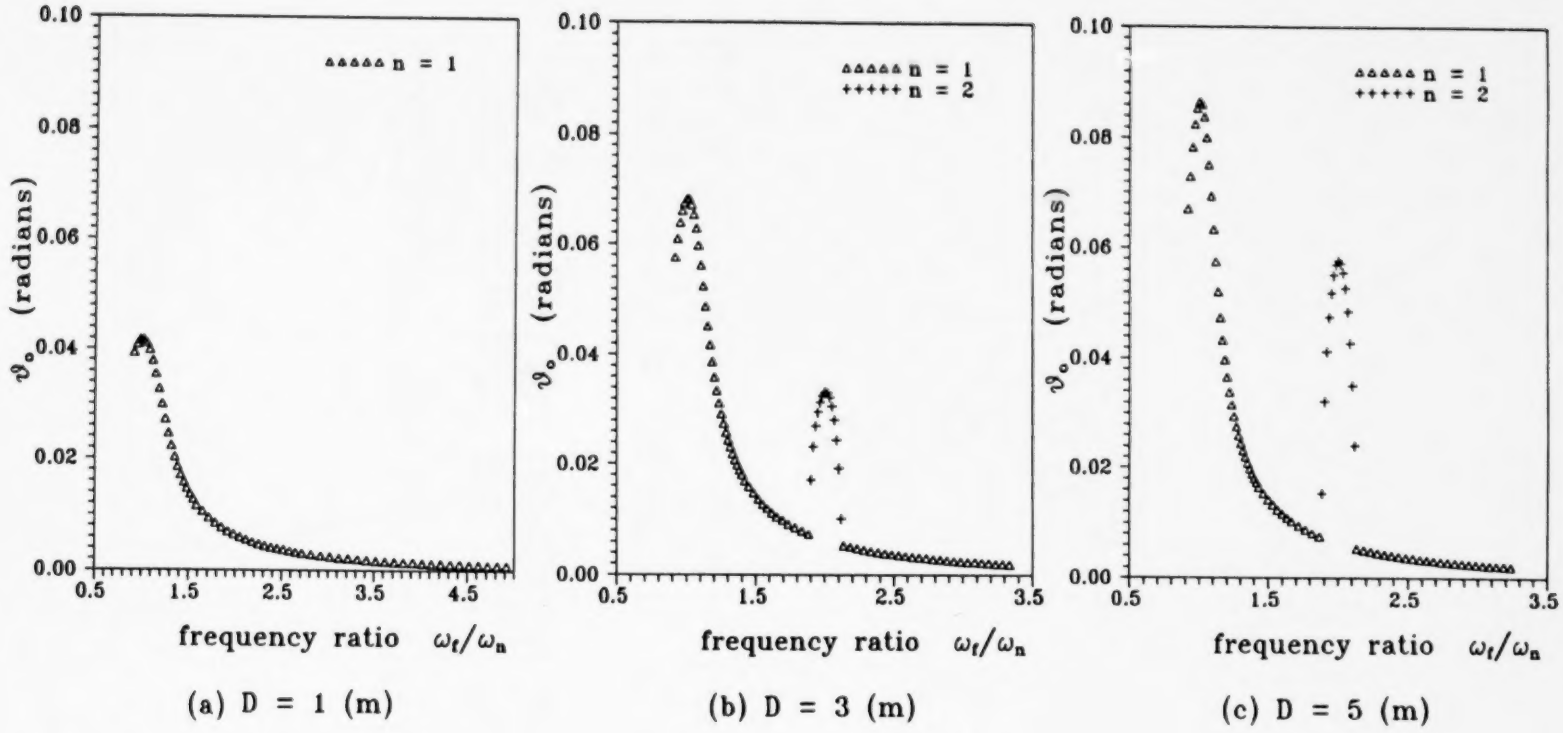


**Figure 4.9:** Frequency response for different values of $D$ with parameter: $d = 100m$, $H = 5m$, $C_m = 2.0$, $C_d = 0.5$, $\beta = 0.5$, $\omega_n = 0.6rad/s$.

decreases significantly when the tower diameter $D$ decreases since decreasing the tower diameter will increase fluid damping significantly. This indicates that large damping can eliminate the existence of complex nonlinear response.

## 4.4 Subharmonic Response

For all values of parameters that have been investigated in this thesis for equation of motion using the total acceleration expression $DU/Dt = \partial U/\partial t + U\partial U/\partial x$, subharmonic response has been observed in most of them. Various subharmonic solutions with different multiples of the forcing period have been seen in frequency response curves for different parameter values. The appearance of the subharmonic solution is a symbol of the qualitative change of the system response. Such a qualitative change is called a bifurcation and can be an indicator of the transition of the system response from order to chaos. Observation and investigation of such solutions are fundamental to identify the route to chaos.

The solutions that the articulated tower system can have in some parameter range for tower diameter $D = 5m$ are listed in Table 4.1. In this table $n$ represents the order of the subharmonic solution and all other parameters are defined before.

It can be seen from this table that as the wave height increases, an increasing number of subharmonic solutions and possibly the chaotic response can appear. Chaotic motion occurs when the drag coefficient $C_d$ is small and the wave height is large. Since values of the drag coefficient are normally in the range from 0.5 to 2.0 for real structures, a drag coefficient of 0.2 is not typical, as mentioned before. This implies that chaotic motion may not be a common phenomenon in a real articulated offshore structure for the parameter range that was investigated here. However chaotic response could occur when wave height is very large for any set of parameter values. The subharmonic response is definitely a common phenomenon for the articulated tower system and it occurs in a variety of parameter range even

**Table 4.1:Solutions for $D = 5m$ using $DU/Dt = \partial U/\partial t + U\partial U/\partial x$**

| H=5 m | | | | | | |
|---|---|---|---|---|---|---|
| | d=100 m | | | d=500 m | | |
| parameters | $C_d = 0.2$ | $C_d = 0.5$ | $C_d = 1.0$ | $C_d = 0.2$ | $C_d = 0.5$ | $C_d = 1.0$ |
| $\beta = 0.2$ | n=1,2,3 | n=1,2 | n=1,2 | n=1 | n=1 | n=1 |
| $\beta = 0.5$ | n=1,2,3 | n=1,2 | n=1,2 | n=1,2 | n=1,2 | n=1 |
| $\beta = 0.7$ | n=1,2,3 | n=1,2 | n=1,2 | n=1,2 | n=1,2 | n=1 |

| H=10 m | | | | | | |
|---|---|---|---|---|---|---|
| | d=100 m | | | d=500 m | | |
| parameters | $C_d = 0.2$ | $C_d = 0.5$ | $C_d = 1.0$ | $C_d = 0.2$ | $C_d = 0.5$ | $C_d = 1.0$ |
| $\beta = 0.2$ | n=1,2,3 | n=1,2,3 | n=1,2 | n=1,2 | n=1,2 | n=1,2 |
| $\beta = 0.5$ | n=1,2,3 | n=1,2,3 | n=1,2 | n=1,2,3 | n=1,2 | n=1,2 |
| $\beta = 0.7$ | n=1,2,3, 6,9,12, chaos | n=1,2,3 | n=1,2 | n=1,2,3 | n=1,2 | n=1 |

| H=20 m | | | | | | |
|---|---|---|---|---|---|---|
| | d=100 m | | | d=500 m | | |
| parameters | $C_d = 0.2$ | $C_d = 0.5$ | $C_d = 1.0$ | $C_d = 0.2$ | $C_d = 0.5$ | $C_d = 1.0$ |
| $\beta = 0.2$ | n=1,2,3, 6,9, chaos | n=1,2,3, 6,12, chaos | n=1,2,3 | n=1,2,3 | n=1,2 | n=1,2 |
| $\beta = 0.5$ | n=1,2,3, 5,6,8, 16,chaos | n=1,2,3, 6,9,12, chaos | n=1,2,3 | n=1,2,3 | n=1,2 | n=1,2 |
| $\beta = 0.7$ | n=1,2,3, 4,5,6,8, 10,16,chaos | n=1,2,3, 6,8, chaos | n=1,2, 4,8 | n=1,2,3 | n=1,2 | n=1 |

**Table 4.2:Solutions for $D = 1m$ using $DU/Dt = \partial U/\partial t + U\partial U/\partial x$**

| d=100 m | | | | | | |
|---|---|---|---|---|---|---|
| H=5 m | | | | H=10 m | | |
| parameters | $C_d = 0.2$ | $C_d = 0.5$ | $C_d = 1.0$ | $C_d = 0.2$ | $C_d = 0.5$ | $C_d = 1.0$ |
| $\beta = 0.2$ | n=1,2 | n=1 | n=1 | n=1,2,4 | n=1 | n=1 |
| $\beta = 0.5$ | n=1,2 | n=1 | n=1 | n=1,2,4 | n=1 | n=1 |
| $\beta = 0.7$ | n=1,2 | n=1 | n=1 | n=1,2 | n=1 | n=1 |

for deeper water depth $d = 500m$ when fluid damping is very large.

The solutions for $D = 1m$ and $D = 3m$ are listed in Tables 4.2 and 4.3 respectively. The same conclusions as above can be drawn from these tables. It also can be seen that complex responses are unlikely to occur when decreasing $D$, as the fluid damping is inversely proportional to the tower diameter $D$.

It has been shown that jump phenomenon often implies the beginning of a period doubling cascade and period doubling often leads to chaotic motion, even though these do not necessarily to occur. Observation of such phenomena is important for identifying chaotic motion.

Shown in Figure 4.10 are two coexisting period three solutions, one with a smaller amplitude (Figure 4.10 (a)) and the other with a larger amplitude (Figure 4.10 (b)) corresponding to a jump phenomenon. Dots in the phase plane diagram represent the Poincaré points. Parameter values for Figure 4.10 are as follows: $d = 100m$, $H = 10m$, $D = 5m$, $C_d = 0.2$, $C_m = 2.0$, $\omega_n = 0.6rad/s$, $\omega_f = 1.77rad/s$, and $\beta = 0.7$. Starting from point $(-0.02, 0.5)$, the motion of the system is attracted to the smaller amplitude solution; while starting from point $(-0.5, 0.5)$, the final motion of the system converges to the larger amplitude solution, indicating the dependence on initial conditions. Power spectra in the right side of each phase plot in Figure 4.10 show that the response is mainly the component with frequency

**Table 4.3:Solutions for $D = 3m$ using $DU/Dt = \partial U/\partial t + U\partial U/\partial x$**

| H=5 m | | | | | | |
|---|---|---|---|---|---|---|
| | d=100 m | | | d=500 m | | |
| parameters | $C_d = 0.2$ | $C_d = 0.5$ | $C_d = 1.0$ | $C_d = 0.2$ | $C_d = 0.5$ | $C_d = 1.0$ |
| $\beta = 0.2$ | n=1,2,3 | n=1,2 | n=1,2 | n=1 | n=1 | n=1 |
| $\beta = 0.5$ | n=1,2,3 | n=1,2 | n=1,2 | n=1,2 | n=1,2 | n=1 |
| $\beta = 0.7$ | n=1,2,3 | n=1,2 | n=1 | n=1,2 | n=1,2 | n=1 |

| H=10 m | | | | | | |
|---|---|---|---|---|---|---|
| | d=100 m | | | d=500 m | | |
| parameters | $C_d = 0.2$ | $C_d = 0.5$ | $C_d = 1.0$ | $C_d = 0.2$ | $C_d = 0.5$ | $C_d = 1.0$ |
| $\beta = 0.2$ | n=1,2,3 | n=1,2 | n=1,2 | n=1,2 | n=1,2 | n=1 |
| $\beta = 0.5$ | n=1,2,3 | n=1,2 | n=1,2 | n=1,2 | n=1,2 | n=1 |
| $\beta = 0.7$ | n=1,2,3, 6,9,12, 15,chaos | n=1,2 | n=1 | n=1,2 | n=1,2 | n=1 |

| H=20 m | | | | | | |
|---|---|---|---|---|---|---|
| | d=100 m | | | d=500 m | | |
| parameters | $C_d = 0.2$ | $C_d = 0.5$ | $C_d = 1.0$ | $C_d = 0.2$ | $C_d = 0.5$ | $C_d = 1.0$ |
| $\beta = 0.2$ | n=1,2,3, 6,chaos | n=1,2,3 | n=1,2 | n=1,2 | n=1,2 | n=1 |
| $\beta = 0.5$ | n=1,2,3, 6,12, chaos | n=1,2,3 | n=1 | n=1,2,3 | n=1,2 | n=1 |
| $\beta = 0.7$ | n=1,2,3, 4,6,7, chaos | n=1,2,3, 3,4,6, 8,chaos | n=1 | n=1,2,3 | n=1,2 | n=1 |

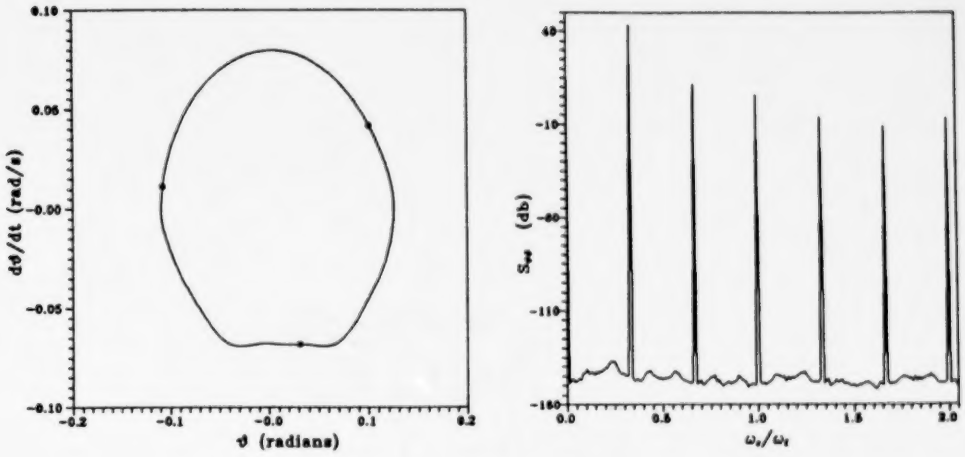


(a) starting point $(-0.02, 0.5)$

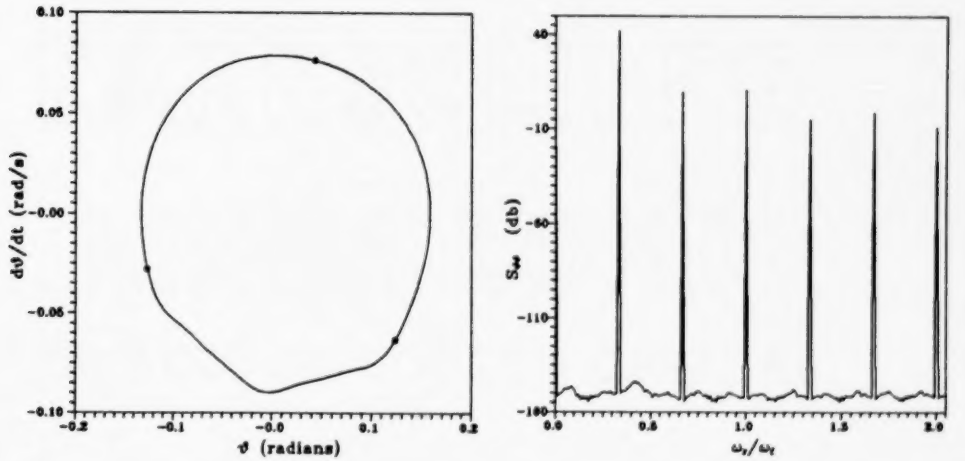


(b) starting point $(-0.5, 0.5)$

**Figure 4.10:** Two coexisting $n = 3$ solutions with parameters: $d = 100m$, $H = 10m$, $D = 5m$, $C_d = 0.2$, $C_m = 2.0$, $\omega_n = 0.6rad/s$, $\beta = 0.7$, $\omega_f = 1.77rad/s$.

equal to 1/3 of the forcing frequency. Figure 4.11 shows a period halving bifurcation from period eight to period four solution with an increase in forcing frequency from $\omega_f = 1.98 rad/s$ to $\omega_f = 1.99 rad/s$. Values of the system parameters for Figure 4.11 are: $d = 100m$, $H = 20m$, $D = 3m$, $C_m = 2.0$, $C_d = 0.5$, $\omega_n = 0.6 rad/s$, and $\beta = 0.7$. If $\omega_f = 1.98 rad/s$, the response is a period eight solution; if $\omega_f$ is increased slightly to $1.99 rad/s$, the response changes to period four solution.

These figures clearly show the dependence of the response on initial conditions and system parameters and asymmetric response of the system.

It has been shown that subharmonic response and coexisting multiple solutions are common for compliant offshore structures. To see the dependence of coexisting solutions on initial conditions, basins of attraction of three coexisting solutions, period one (n=1), period three (n=3), and period six solution (n=6), are plotted in Figure 4.12. System parameter values for this figure are: $d = 100m$, $H = 10m$, $D = 5m$, $C_d = 0.2$, $C_m = 2.0$, $\omega_n = 0.6 rad/s$, $\omega_f = 1.8 rad/s$, and $\beta = 0.7$. The step size of this map for both axes, the initial tower angular displacement $\theta$ and initial angular velocity $\dot{\theta}$, is 0.0025 and 27,889 different initial conditions in total have been used. The motion starting from $n = 1$ regions will be attracted to period one solution. Similarly, the motion starting from $n = 3$ regions will finally converge to the period three solution, and so on. The final motion that system settles down only depends on the initial conditions. As can be seen in this map the shape of basins of attraction is very complicated and the stretching and folding effects are clearly shown. For the case of the parameters used here, basin boundaries appear as smooth, continuous lines, implying that if the motion starts away from the boundary, small uncertainties in them will not affect the final response. However, it has been shown in many nonlinear systems that, in general, the basin boundaries are not smooth and have a fractal nature (see for example, Kapitaniak [41]). In this case, any small uncertainties in initial conditions may lead to uncertainties in the outcome of the system. As the step size becomes smaller and smaller, the initial

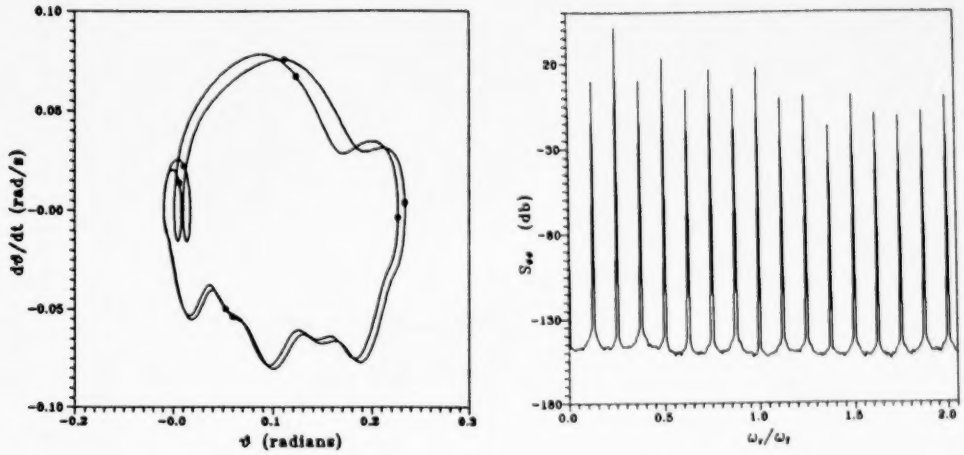


(a) $\omega_f = 1.98\ rad/s$

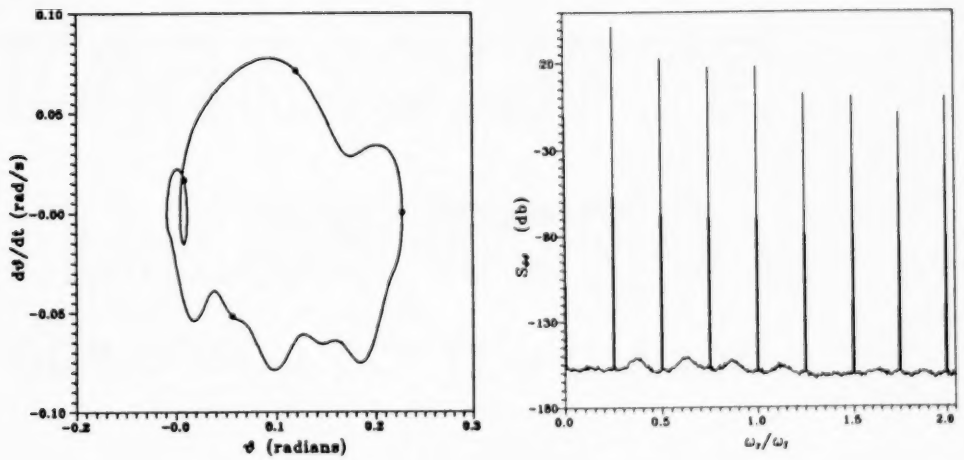


(b) $\omega_f = 1.99\ rad/s$

**Figure 4.11:** Period halving bifurcation with parameters: $d = 100m$, $H = 20m$, $D = 3m$, $C_m = 2.0$, $C_d = 0.5$, $\omega_n = 0.6 rad/s$, $\beta = 0.7$.

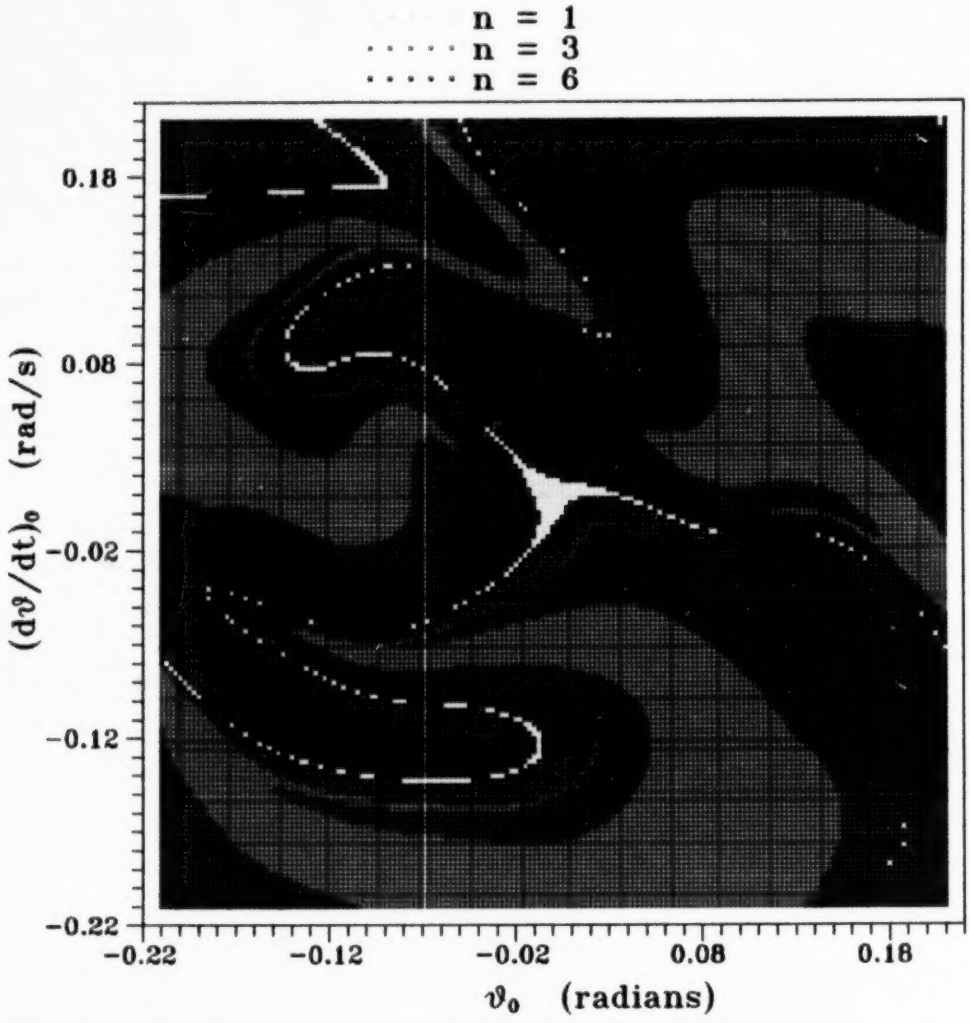


Figure 4.12 Basins of attraction

parameters: d=100m, H=10m, $C_d$=0.2, $C_m$=2, $\omega_n$=0.6rad/s, $\omega_f$=1.8rad/s, $\beta$=0.7, D=5m

condition map will show a finer and finer structure on the boundaries. Existence of fractal basin boundaries shows that even a system with periodic response can exhibit a sensitive dependence on initial conditions. This makes the dynamic response of such structures difficult to predict.

## 4.5 Bifurcation to Chaos

To further investigate the frequency response curve of the articulated tower and to identify the route to chaos by period doubling bifurcation, here, as an example, the frequency response curve for the case previously shown in Figure 4.1 (b) will be discussed in detail. For the frequency ratio range that has been investigated here, there are three main frequency ratio regions, each of them being associated with a resonant peak. The solutions are all period one solution in the range of frequency ratio from 0.9 to about 1.7 with the first resonant peak value (the fundamental resonance) being about 0.15 *radians* at a frequency ratio of about 1.0. In the next frequency ratio range from about 1.7 to 2.4, the period of solution is twice of that of the forcing, and hence they are period two solutions. Following this frequency range is a period one solution range with very small mean response amplitude. In the frequency ratio range from 2.6 to 3.3 corresponding to the next subharmonic resonance, various subharmonic solutions, period three, period six, and period twelve solutions, are observed. At $\omega_f/\omega_n = 2.9$, there exist two different period three solutions and a jump phenomenon is clearly seen at this value of frequency ratio. The period of response changes to different multiples of the period of excitation after this value of frequency ratio. An infinite period doubling cascade is formed and the solution eventually becomes chaotic in the range $\omega_f/\omega_n = 3.0 \sim 3.1$. Note also that at the higher frequency range period one solutions coexist with the subharmonic solutions.

To see changes in response period clearly, the Poincaré points for each value of forcing frequency corresponding to this period doubling are plotted in Fig-

ure 4.13. This bifurcation diagram shows the global bifurcations of the system response for increasing forcing frequency. As can be seen in this figure, period three solution bifurcates to period six solution at about $\omega_f = 1.766\ rad/s$. At about $\omega_f = 1.775\ rad/s$ the response period doubles again and period twelve solution is born. Then period twelve solution changes to period six solution, forming an incomplete Feigenbaum cascade (see for example, Thompson [8]). The period doubling begins again at about $\omega_f = 1.819\ rad/s$ and the period six solution bifurcates to give the birth of new solution with doubled period. As this period doubling continues the response of the system finally becomes chaotic when forcing frequency is about 1.8275.

Also the period doubling phenomenon can be seen from a sequence of Poincaré maps and power spectra shown in Figures 4.14 (a)-(h). These figures clearly show changes in the response period when varying forcing frequency $\omega_f$, and the period doubling route to chaos.

The last Poincaré map for $\omega_f = 1.83\ rad/s$ given in Figure 4.15 shows a chaotic response in which 2000 Poincaré points have been computed and plotted after 1000 forcing cycles transients. The power spectrum corresponding to each Poincaré map is shown on the right side of each map and is plotted as a function of nondimensional frequency ratio, $\omega_r/\omega_f$, the ratio of the response frequency to the forcing frequency. For the periodic response the power spectrum consists of a sequence of spikes at frequencies of $(m/n)\omega_f$, where $m = 1,\ 2,\ 3, \ldots,\ n$ is the order of subharmonic solution. Thus for the solution of order $n$, there are $n$ spikes within the frequency ratio range from 0 to 1. For chaotic response, the power spectrum is continuous, showing "random like" behaviour as in Figure 4.15. The chaotic attractor, as can be seen in Figure 4.15, is a narrow one as the damping of the system in this case is very small.

A universal feature of period doubling cascade discovered by Feigenbaum [33] is the so-called Feigenbaum number. The Feigenbaum number associated with this

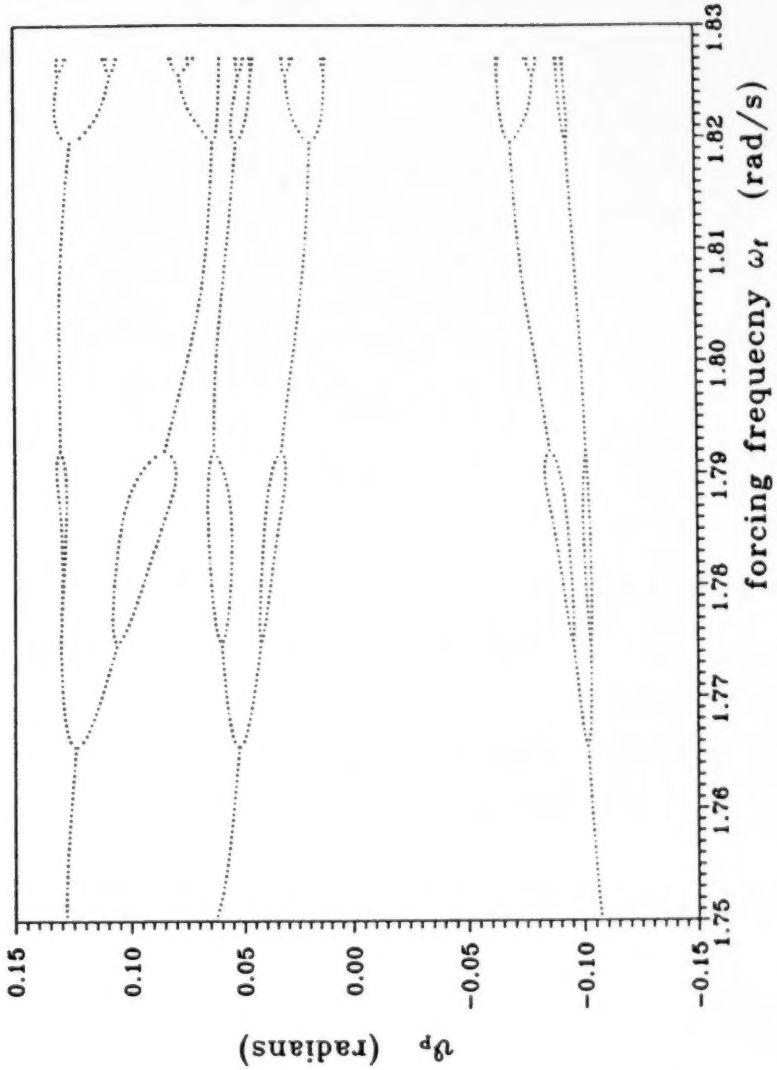


**Figure 4.13:** Bifurcation diagram with parameters: $d = 100m$, $H = 10m$, $D = 3m$, $C_m = 2.0$, $C_d = 0.2$, $\omega_n = 0.6rad/s$, $\beta = 0.7$.

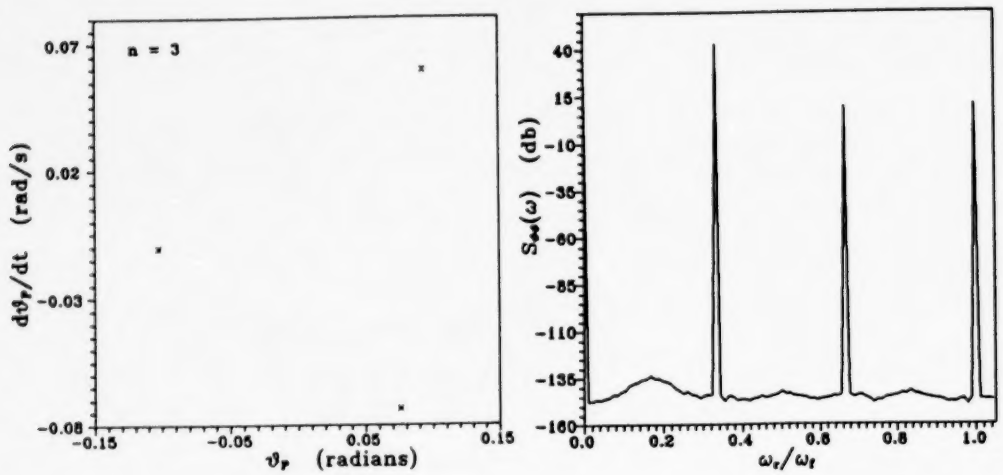


(a) $\omega_f = 1.76\ rad/s$, period 3 solution

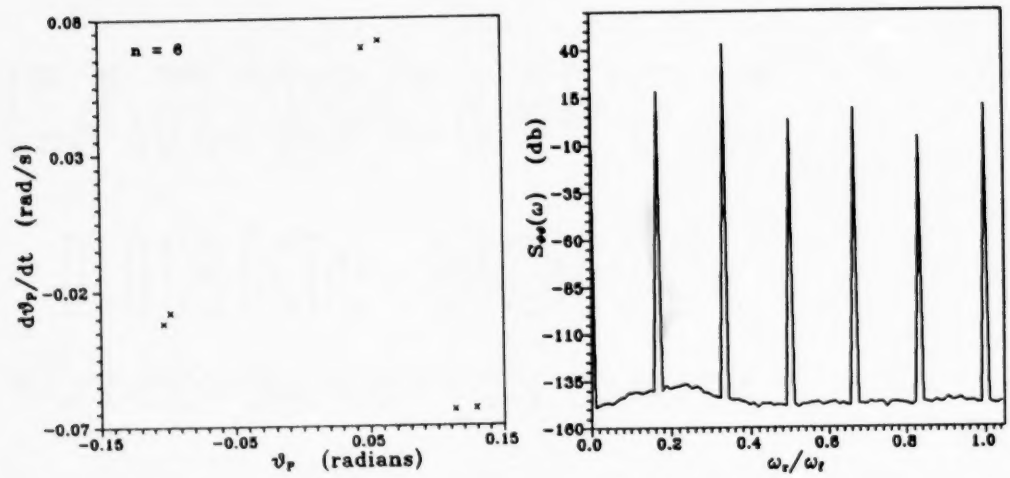


(b) $\omega_f = 1.77\ rad/s$, period 6 solution

**Figure 4.14:** Poincaré maps and power spectra

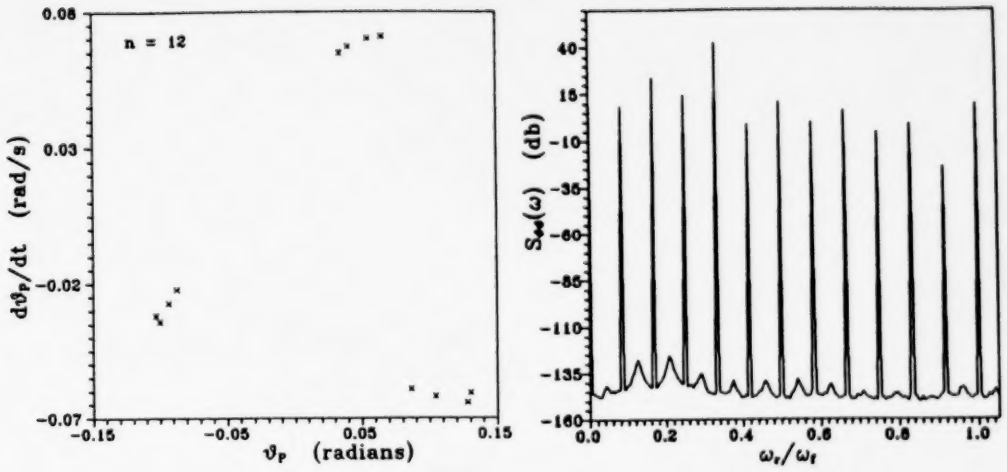


(c) $\omega_f = 1.792\ rad/s$, period 12 solution

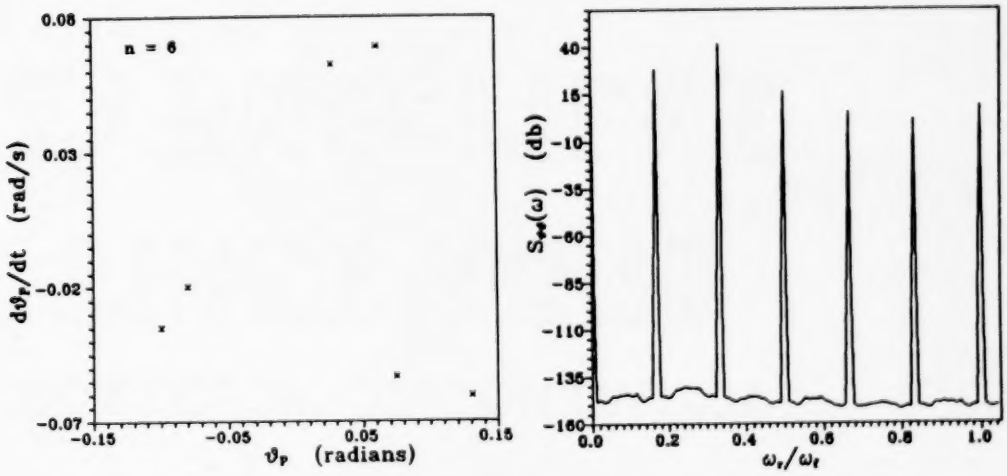


(d) $\omega_f = 1.80\ rad/s$, period 6 solution

**Figure 4.14:** Poincaré maps and power spectra (cont'd)

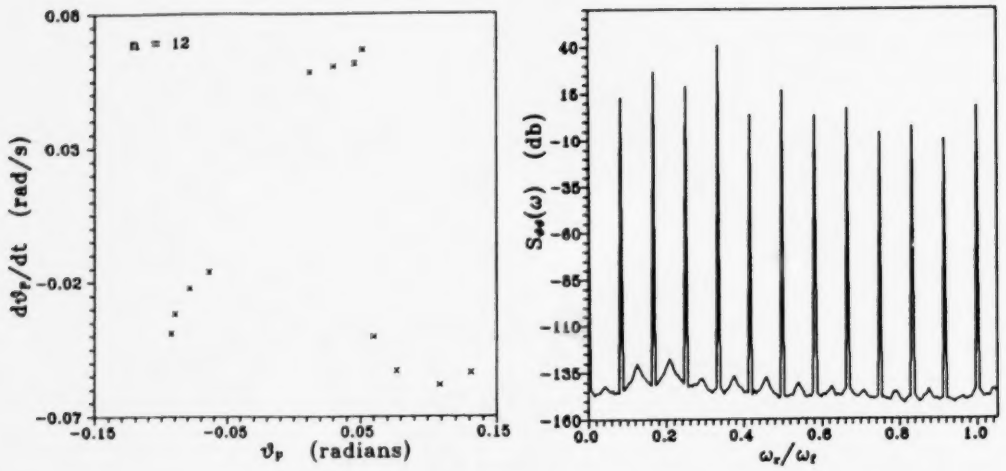


(e) $\omega_f = 1.825\ rad/s$, period 12 solution

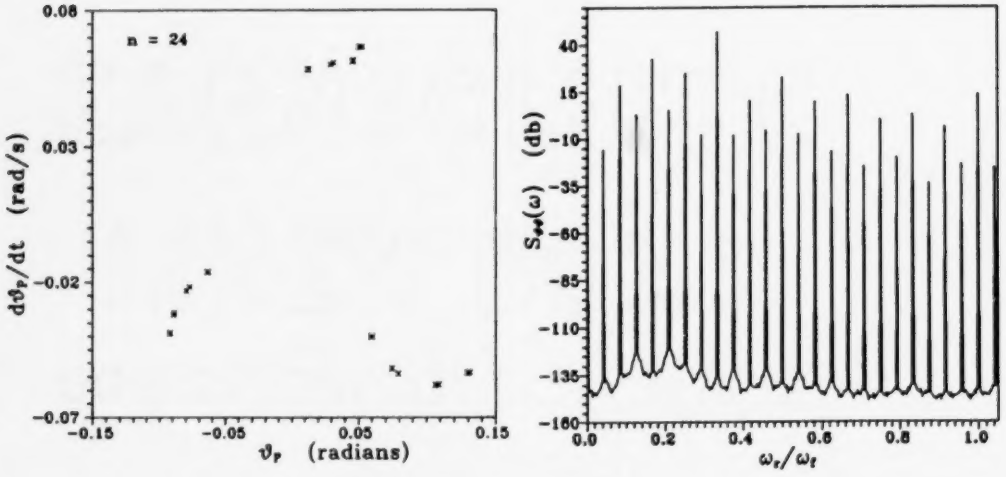


(f) $\omega_f = 1.826\ rad/s$, period 24 solution

**Figure 4.14:** Poincaré maps and power spectra (cont'd)

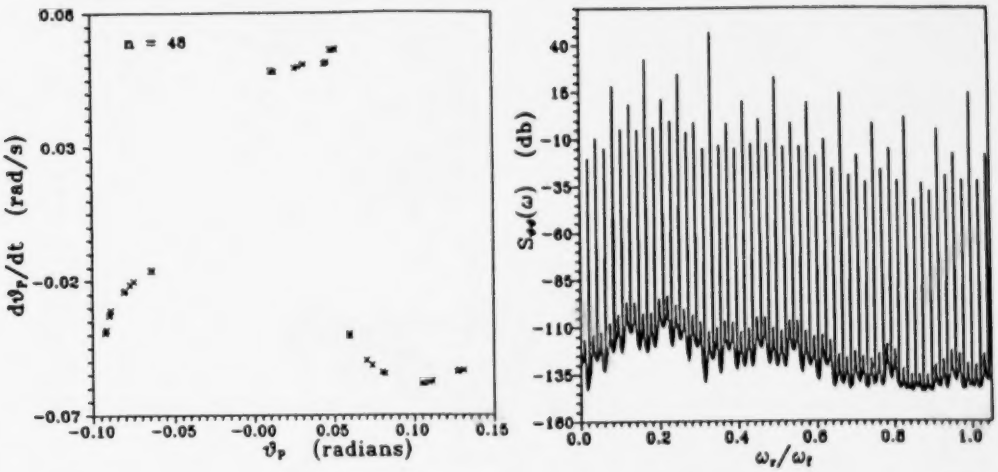


(g) $\omega_f = 1.82715\ rad/s$, period 48 solution

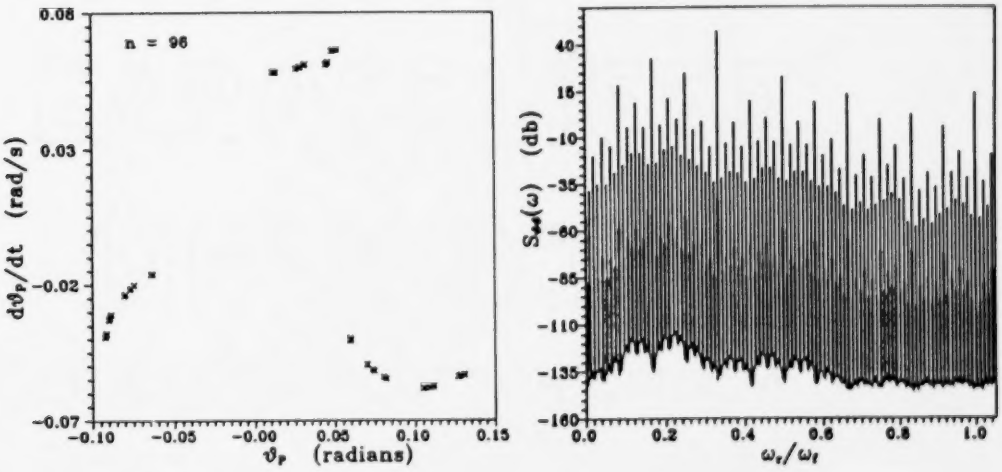


(h) $\omega_f = 1.8272\ rad/s$, period 96 solution

**Figure 4.14:** Poincaré maps and power spectra (cont'd)

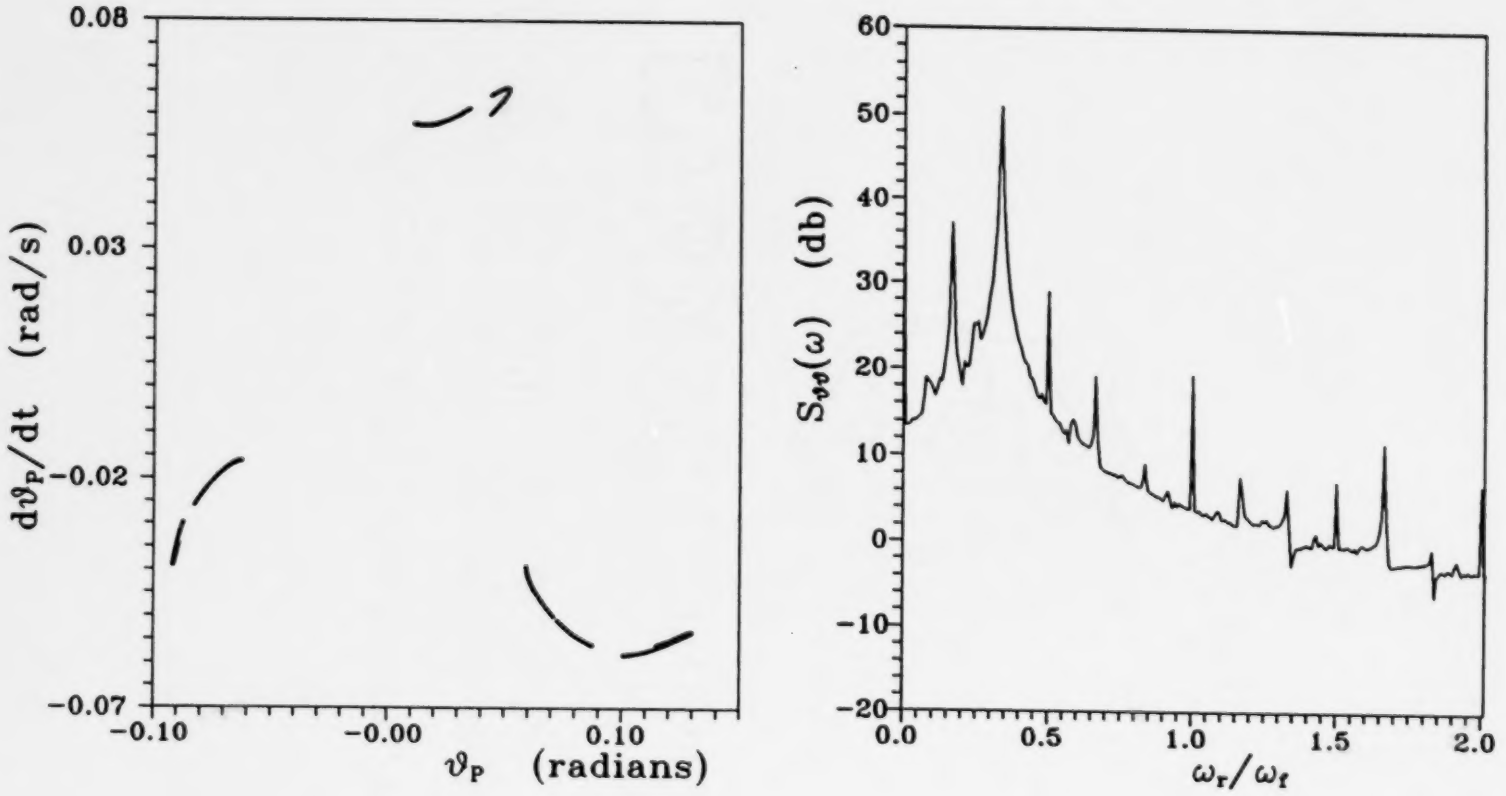


$\omega_f = 1.83$ (rad/s)

**Figure 4.15:** Poincaré map and power spectrum for chaotic response

period doubling bifurcation which leads to chaotic response has also been calculated approximately and one bifurcation branch in Figure 4.13 has been enlarged and shown in Figure 4.16. These computed Feigenbaum numbers are

$$\delta_1 = \frac{\Delta\omega_{f12}}{\Delta\omega_{f24}} = 4.873,\ \delta_2 = \frac{\Delta\omega_{f24}}{\Delta\omega_{f48}} = 4.760,\ \delta 3 = \frac{\Delta\omega_{f48}}{\Delta\omega_{f96}} = 4.649. \qquad (4.4)$$

It can be seen that these values show the gradual convergence to the universal Feigenbaum number of 4.66920..., which is obtained for the logistic equation and has also been observed in various nonlinear systems and experimental studies. It also can be expected that, with this fixed ratio, the bifurcation cascade will finally reach an accumulation point where the observed chaotic response occurs.

## 4.6 Numerical Calculation of Liapunov Exponent

The existence of a solution with arbitrarily long period does not necessarily imply chaotic motion. The defining characteristic of a chaotic system is its sensitive dependence on initial conditions. As discussed before, the Liapunov exponent is used as a quantitative test of the divergence of nearby starting points and measures the sensitivity of the system to changes in initial conditions. Since the system considered here is a second order dissipative differential system, there are three Liapunov exponents for this system, one is negative to ensure that the system is dissipative, and one has to be zero since there is no stretching, contracting and folding in the direction of time axis in phase space for a periodically driven system. Thus the sign of the largest nonzero Liapunov exponent will decide whether the response of a system is chaotic or not. If the largest nonzero Liapunov exponent is positive, this implies chaotic response, whereas if the largest nonzero Liapunov exponent is negative, indicates periodic response.

The algorithm used to calculate the largest nonzero Liapunov exponent here is by using variational equations of original differential equation. The variational

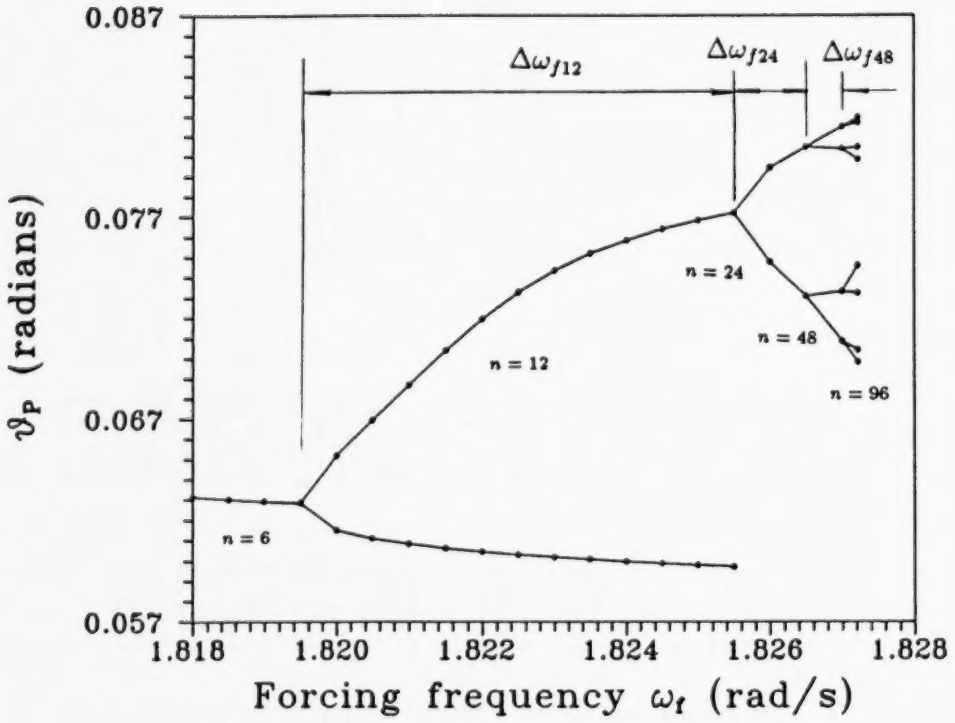


**Figure 4.16:** Partial enlargement of bifurcation diagram

equations relate the initial divergence to the evolved divergence after a short time in phase space by linear combination. The largest nonzero Liapunov exponent can be obtained by solving the variational equations. Further details about this method are given in Appendix B, or references [5, 36].

Here the largest nonzero Liapunov exponent has been calculated for the system parameter values associated with observed chaotic motion indicated previously in Figure 4.15. Figure 4.17 shows the time evolution of the largest Liapunov exponent as a function of the number of forcing cycles. The total time used to calculate the largest nonzero Liapunov exponent is 500 forcing cycles after transients have died out. The forcing frequency $\omega_f$ in Figure 4.17 is 1.83 $rad/s$. Motion starting from initial point $\theta = 0.1 radians$, $\dot{\theta} = 0.0 rad/s$ is attracted to chaotic motion and the corresponding largest nonzero Liapunov exponent is positive as shown in Figure 4.17 (a), indicating the sensitive dependence on initial conditions.

The computed positive largest nonzero Liapunov exponent further verifies the observed chaotic response. Note that observed chaotic motion coexists with period one solution (see Figure 4.1 (b)). The largest nonzero Liapunov exponent for coexisting period one solution, with initial conditions $\theta = 0 radians$ and $\dot{\theta} = 0 rad/s$, is also calculated as shown in Figure 4.17 (b). The negative exponent in this case implies the convergence to periodic motion, in this case the period one solution.

It should be mentioned here that some results of numerical calculation of the Liapunov exponent were not consistent with its definition, especially when the system response is very close to a bifurcation point. For example, the calculated largest nonzero Liapunov exponent, which should be negative and close to zero for the periodic motion shown in Figure 4.1 (b), was positive at $\omega_f = 1.02 rad/s$ ($\omega_f/\omega_n = 1.7$) and $\omega_f = 1.42 \sim 1.43 rad/s$ ($\omega_f/\omega_n = 2.37 \sim 2.38$), with other system parameter values being shown in Figure 4.1. The system response in both cases is near a bifurcation point with the first case being from period one solution to period two solution and the second from period two solution to period one solution. Although

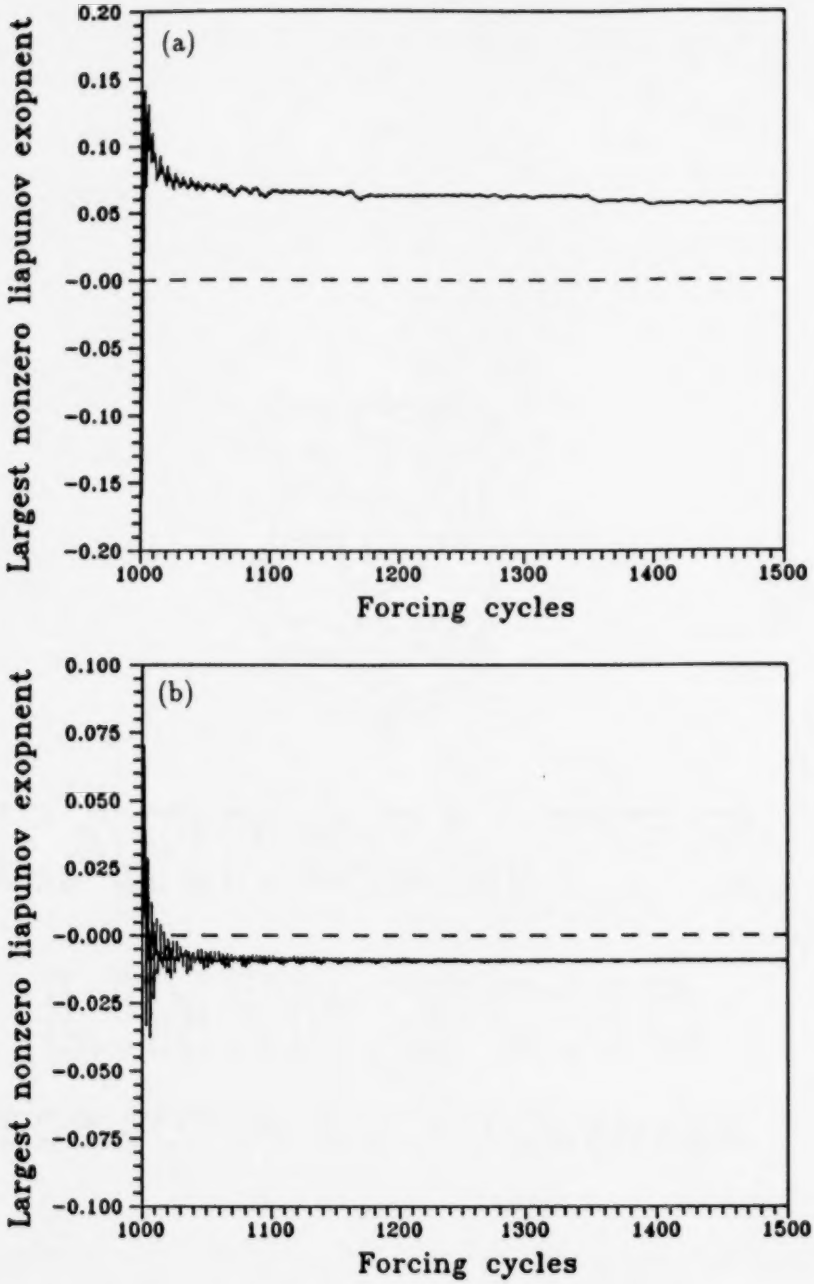


**Figure 4.17:** Time evolution of the largest nonzero Liapunov exponent. (a) For chaotic response; (b) For periodic response.

the computed Liapunov exponent was positive, it was observed from time history that the response was not chaotic but periodic. A common nature for these two cases is that the response amplitude is very small and it takes very long time to converge to steady state. The reason for this discrepancy could result from an error in the computer program. For this reason the program has been checked with a number of well known nonlinear systems, such as Duffing's equation [5], Van der Pol's equation [41], and a driven pendulum system given by Baker [42]. The calculated Liapunov exponents in each case were in good agreement with the results shown in above mentioned references. Much effort has also been made to test the computer program of calculating the Liapunov exponent by varying parameters, such as the total number of forcing cycles, initial length of the principal axis, as well as the Liapunov time step size. However, the calculated Liapunov exponent was found to be independent of these parameters and showed very good convergence in all cases. Despite these program checks the reasons for the calculated Liapunov exponent being not consistent with the type of motion that the system really experiences are as yet unknown. Problems in calculating the Liapunov exponents have also been reported by Plaschko et al. [43], who studied the transition of a flow-induced cylinder vibration system. Further work is needed to find out the reasons for this inconsistency. For reference the method used to calculate the largest Liapunov exponent is given in Appendix B.

# Chapter 5

# Summary and Conclusions

A single-degree-of-freedom model of the articulated tower subjected to regular wave excitation is studied in this thesis. Linear wave theory and the relative velocity formulation of the Morison equation have been used to obtain the wave forces acting on the structure. The exact form of the fluid force is retained so that the model presented here can better represent actual fluid loading. The resulting equation of motion is nonlinear in both the drag force and wave exciting forces when the total acceleration of fluid particle is used. The drag force is a nonlinear quadratic function of the relative velocity between the fluid particle and tower. The amplitude of wave exciting forces is a nonlinear function of the tower angular displacement so that the resulting equation of motion of the articulated tower system is actually a combined parametric and external excitation system in this case. In order to study the influence of each nonlinearity arising in the equation of motion on the system behaviour, the local expression of fluid particle acceleration is used so that the nonlinear quadratic drag force is the only nonlinearity in equation of motion. Thus different equations of motion have been considered each with a different form of the fluid particle acceleration. An Adams-Bashforth-Moulton numerical method has been used to obtain the solutions of different equations of motion. A large variety

of system parameters has been investigated to provide a basic understanding of the behaviour of this compliant articulated tower.

It has been found that the nonlinear wave exciting force, arising from the nonlinear convective terms in wave kinematics, plays a crucial role in the complex behaviour in the system parameter range investigated here. Over two hundred cases with different sets of system parameters have been investigated using the local form of fluid acceleration. When the local form is used, the nonlinear drag force is the only nonlinearity in the system and it is significant to note that subharmonic or chaotic responses have not been found yet in this case. It seems that complex nonlinear responses are unlikely to occur when the inertia forcing terms corresponding to the convective terms are neglected. This is in contrast to the results of Gottlieb et al. [27]. It may be that the proper combination of the system parameters to observe complex response and chaotic response has not yet been considered.

For the system parameter range that has been studied here, chaotic response was found when the drag coefficient is small and wave height is large. This occurs for cases that $DU/Dt = \partial U/\partial t + U\partial U/\partial x$ is used to evaluate the fluid particle acceleration. Since the drag coefficient for real structures typically is much larger than those where chaos has been found in this thesis, the chaos is probably not a common phenomenon for real structures except when the wave height is very large. Alternatively, when $DU/Dt = \partial U/\partial t + (U - \dot{x})\partial U/\partial x$ is used, the numerical simulations have shown that chaotic response may occur at slightly larger values of the drag coefficient and slightly smaller wave heights. Thus when either form of the total acceleration expressions considered in this thesis is used, nonlinear response can be anticipated. It is felt that inclusion of convective terms in the expression for the fluid particle acceleration is required to accurately model the fluid kinematics. This is the case even when the magnitude of the tower oscillation is small. It has also been shown that the nonlinear convective terms only affect the system response in the subharmonic frequency range and does not significantly affect the

system response in the fundamental resonant frequency range.

In a hundred and thirty cases of system parameters, subharmonic response has been observed in most of them. Thus the subharmonic response is definitely a common phenomenon for the articulated tower. Various subharmonic responses with multiples of the forcing period can occur for different values of system parameters.

Numerical simulations have shown that the stability of solutions to the equation of motion is sensitive to the amplitude of the wave exciting force. Since wave height contributes mainly to the amplitude of this wave exciting force, the solution changes qualitatively with increasing wave height. For large wave height, the secondary resonances may be unstable and various nonlinear phenomena such as jump phenomenon, coexistence of multiple competing steady state solutions, finite and infinite period doubling, and chaos can occur. For small wave height, subharmonic response may also occur but jump phenomenon and period doubling are unlikely to occur. This implies that wave height is an important parameter influencing the system behaviour as might be expected.

The fluid damping is another important factor which significantly influences behaviour of the articulated tower system. The large fluid damping provided by a large drag coefficient can eliminate the appearance of possible nonlinear responses and nonlinear phenomena if it is large enough. The nonlinear responses diminish or totally disappear as the nonlinear wave exciting effect becomes damped out by large fluid damping increasing with water depth. Therefore the system is more stable with increasing water depth. However, as already discussed, the model presented in this thesis may not appropriate to represent the dynamics of the real structures in very deep water, as the deformation of the articulated tower could then be significant and could not be neglected. Further investigation for the articulated tower systems which includes the tower deformation will be necessary for these cases.

The model for the articulated tower system presented in this thesis better rep-

resents the actual dynamic behaviour of such structure. The assumptions that have been made for this structure are proper and realistic. Numerical simulations are very tedious and time consuming since the same procedure needs to be performed for each set of system parameters. Further investigation of stability analysis is needed by employing analytical methods to guide the study of nonlinear behaviour of the articulated tower system.

# References


[1] Lee, G. C., " Recent Advances in Design and Construction of Deepwater Platforms, Part 1 ", *Ocean Industry*, pp. 71-88, November, 1980.

[2] Thornton, D., "A General Review of Future Problems and Their Solution", *Proceedings of Second International Conference on Behaviour of Offshore Structures*, London, pp. 773-782, 1979.

[3] Patel, M. H., *Dynamics of Offshore Structures*, Butterworths, 1989.

[4] Isaacson, M., " Recent Developments In the Computation of Nonlinear Wave Interactions with Offshore Structures ", *The Speciality Conference on Computer Methods in Offshore Engineering*, Halifax, Canadian Society for Civil Engineering, pp. 73-97, 1984.

[5] Moon, F. C., *Chaotic Vibrations: An Introduction for Applied Scientists and Engineers*, John Wiley & Sons, 1987.

[6] Morison, J. R., O'Brien, M. P., Johnson, J. W. and Schaff, S. A., " The Force Exerted by Surface Waves on Piles ", *Transactions of the American Institute of Mining and Metallurgical Engineers*, Vol. 189, pp. 149-154, 1950.

[7] May, R. M.,"Simple Mathematical Models with Very Complicated Dynamics", *Nature*, Vol. 261, pp. 459-467, June, 1976.

[8] Thompson, J. M. T. and Stewart, H. B., *Nonlinear Dynamics and Chaos: Geometric Methods for Engineers and Scientists*, John Wiley & Sons, 1986.

[9] Bishop, S. R. and Virgin, L. N., " The Onset of Chaotic Motions of a Moored Semi-submersible", *Journal of Offshore Mechanics and Arctic Engineering*, ASME, Vol. 110, pp. 205-209, August, 1988.

[10] Gottlieb, O., " Bifurcations and Routes to Chaos in Wave-Structure Interaction Systems ", *Journal of Guidance, Control, and Dynamics*, Vol. 15, No. 4, pp. 832-839, July-August, 1992.

[11] Thompson, J. M. T., Bokaian, A. R. and Ghaffari, R., " Subharmonic and Chaotic Motions of Compliant Offshore Structures and Articulated Mooring Towers ", *Journal of Energy Resources Technology*, ASME, Vol. 106, pp. 191-198, June, 1984.

[12] Sarpkaya, T. and Isaacson, M., *Mechanics of Wave Forces on Offshore Structures*, Van Nostrand Reinhold, 1981.

[13] Chakrabarti, S. K., " Recent Advances in High Frequency Wave Forces ", *Proceedings of Fourth International Offshore Mechanics and Arctic Engineering Symposium*, Vol. 1, pp. 125-141, Dallas, Texas, 1985.

[14] Keulegan, B. P. and Carpenter, L. H., " Forces on Cylinders and Plates in an Oscillating Fluid ", *Journal of Research of the National Bureau of Standards*, Vol. 60, No. 5, pp. 423-440, 1958.

[15] Chakrabarti, S. K. and Cotter, D., " Hydrodynamic Coefficients of a Mooring Tower ", *Journal of Energy Resources Technology*, ASME, Vol. 106, pp. 183-190, June, 1984.

[16] Williamson, C. H. K., " In-line Response of a Cylinder in Oscillatory Flow ", *Applied Ocean Research*, Vol. 7, No. 2, pp. 97-106, 1985.

[17] Koterayama, W. and Nakamura, M., " Wave Forces Acting on a Moving Cylinder", *Journal of Offshore Mechanics and Arctic Engineering*, ASME, Vol. 110, pp. 315-319, November, 1988.

[18] Newman, J. N., *Marine Hydrodynamics*, The MIT Press, 1977.

[19] Spanos, P.-T. and Chen, T. W., " Response of a Dynamic System to Flow-Induced Load ", *International Journal of Non-Linear Mechanics*, Vol. 15, pp. 115-125, 1980.

[20] McNamara, J. F. and Lane, M., "Practical Modelling for Articulated Risers and Loading Columns", *Journal of Energy Resources Technology*, ASME, Vol. 106, pp. 444-450, December, 1984.

[21] Chakrabarti, S. K. and Cotter, D. C., " Motions of Articulated Towers and Moored Floating Structures", *Journal of Offshore Mechanics and Arctic Engineering*, ASME, Vol. 111, pp. 233-241, August, 1989.

[22] Lipsett,A. W., *Nonlinear Response of Structures to Regular and Random Waves*, Ph. D. Dissertation, University of British Columbia, 1985.

[23] Yagasaki, K., " Chaos in a Weakly Nonlinear Oscillator with Parametric and External Resonances", *Journal of Applied Mechanics*, ASME, Vol. 58, pp. 244-250, March, 1991.

[24] Yagasaki, K., Sakata, M. and Kimura, K., " Dynamics of a Weakly Nonlinear System Subjected to Combined Parametric and External Excitation", ASME, Vol. 57, pp. 209-217, March, 1990.

[25] HaQuang, N., Mook, D. T. and Plaut, R. H., " A Non-linear Analysis of the Interactions Between Parametric and External Excitations", *Journal of Sound and Vibration*, Vol. 118, pp. 425-439, 1987.

[26] Choi, H. S. and Lou, J. Y. K., " Nonlinear Behaviour of an Articulated Offshore Loading Platform ", *Applied Ocean Research*, Vol. 13, No. 2, pp. 63-74, 1991.

[27] Gottlieb, O. , Yim, S. C. S. and Hudspeth, R. T., " Analysis of Nonlinear Responses of an Articulated Tower ", *Proceedings of the First International Offshore and Polar Engineering Conference*, pp. 384-390, Edinburgh, 1991.

[28] Liaw, C. Y., " Chaotic and Periodic Responses of a Coupled Wave-Force and Structure System ", *Computers and Structures*, Vol. 30, No. 4, pp. 985-993, 1988.

[29] Fujino, M. and Sagara, N., "An Analysis of Dynamic Behaviour of an Articulated Column in Waves - Effects of Nonlinear Hydrodynamic Drag Force on the Occurrence of Subharmonic Oscillation ", *Journal of the Society of Naval Architects of Japan*, pp. 103-112, 1990 (in Japanese).

[30] Nayfel, A. H. and Khdeir, A. A., " Nonlinear Rolling of Ships in Regular Beam Seas", *International Shipbuilding Progress*, Vol. 33, pp. 40-49, 1986.

[31] Nayfel, A. H. and Khdeir, A. A., " Nonlinear Rolling of Biased Ships in Regular Beam Waves", *International Shipbuilding Progress*, Vol. 33, pp. 84-93, 1986.

[32] Liaw, C. Y., " Numerical Modelling and Subharmonic Bifurcations of a Compliant Cylinder Exposed to Waves ", *Journal of Offshore Mechanics and Arctic Engineering*, ASME, Vol. 111, pp. 29-36, February, 1989.

[33] Feigenbaum, M. J., " Quantitative Universality for a Class of Nonlinear Transformations ", *Journal of Statistical Physics*, Vol. 19, No. 1, pp. 25-52, 1978.

[34] Feigenbaum, M. J., " Universal Behaviour in Nonlinear Systems ", *Physica*, Vol. 9D, pp. 433-438, 1983.

[35] Haken, H., " At Least One Lyapunov Exponent Vanishes if the Trajectory of an Attractor Does Not Contain a Fixed Point", Physics Letters, Vol. 94A, pp. 71-72, 1983.

[36] Wolf, A., Swift, J. B., Swinney, H. L. and Vastano, J. A., " Determining Lyapunov Exponents From a Time Series ", *Physica*, Vol. 16D, pp. 285-317, 1985.

[37] Press, W. H., Flannery, B. P., Teukosky, S. A. and Vettering, W. T., *Numerical Recipes: The Art of Scientific Computing (FORTRAN version)*, Cambridge University Press, 1989.

[38] Isaacson, M., " Nonlinear Inertia Forces on Bodies ", *Journal of the Waterway, Port, Coastal and Ocean Division*, ASCE, Vol. 105, No. WW3, pp. 213-227, August, 1979.

[39] Piessens, R., de Doncker-Kapenga, E., Uberhuber, C. W. and Kahaner, D. K., *QUADPACK: A Subroutine Package for Automatic Integration*, Springer-Verlag, 1983.

[40] Shampine, L. F. and Gordon, M. K., *Computer Solution of Ordinary Differential Equations*, W. H. Freeman and Company, 1975.

[41] Kapitaniak, T., *Chaotic Oscillations in Mechanical Systems*, Manchester University Press, 1991.

[42] Baker, G. L. and Gollub, J. P., *Chaotic Dynamics: an introduction*, Cambridge University Press, 1990.

[43] Plaschko, P., Berger, E. and Brod, K., " The Transition of Flow-Induced Cylinder Vibrations to Chaos ", *Nonlinear Dynamics: An International Journal of Nonlinear Dynamics and Chaos in Engineering Systems*, Vol. 4, No. 3, June, pp. 251-268, 1993.

# Appendix A

# Solutions Using Local Acceleration Only

Shown in this Appendix are tables which list possible solutions in a variety of the system parameters that have been investigated in this thesis for using local form of fluid particle acceleration $DU/Dt = \partial U/\partial t$.

The results show that complex responses of the articulated tower system are unlikely to occur if the local acceleration only is used to evaluate the fluid particle acceleration.

**Table A.1:Solutions for $D = 5m$ using $DU/Dt = \partial U/\partial t$**

| H=5 m | | | | | | |
|---|---|---|---|---|---|---|
| | d=100 m | | | d=500 m | | |
| parameters | $C_d = 0.2$ | $C_d = 0.5$ | $C_d = 1.0$ | $C_d = 0.2$ | $C_d = 0.5$ | $C_d = 1.0$ |
| $\beta = 0.2$ | n=1 | n=1 | n=1 | n=1 | n=1 | n=1 |
| $\beta = 0.5$ | n=1 | n=1 | n=1 | n=1 | n=1 | n=1 |
| $\beta = 0.7$ | n=1 | n=1 | n=1 | n=1 | n=1 | n=1 |
| H=10 m | | | | | | |
| | d=100 m | | | d=500 m | | |
| parameters | $C_d = 0.2$ | $C_d = 0.5$ | $C_d = 1.0$ | $C_d = 0.2$ | $C_d = 0.5$ | $C_d = 1.0$ |
| $\beta = 0.2$ | n=1 | n=1 | n=1 | n=1 | n=1 | n=1 |
| $\beta = 0.5$ | n=1 | n=1 | n=1 | n=1 | n=1 | n=1 |
| $\beta = 0.7$ | n=1 | n=1 | n=1 | n=1 | n=1 | n=1 |
| H=20 m | | | | | | |
| | d=100 m | | | d=500 m | | |
| parameters | $C_d = 0.2$ | $C_d = 0.5$ | $C_d = 1.0$ | $C_d = 0.2$ | $C_d = 0.5$ | $C_d = 1.0$ |
| $\beta = 0.2$ | n=1 | n=1 | n=1 | n=1 | n=1 | n=1 |
| $\beta = 0.5$ | n=1 | n=1 | n=1 | n=1 | n=1 | n=1 |
| $\beta = 0.7$ | n=1 | n=1 | n=1 | n=1 | n=1 | n=1 |
| H=30 m | | | | | | |
| | d=100 m | | | d=500 m | | |
| parameters | $C_d = 0.2$ | $C_d = 0.5$ | $C_d = 1.0$ | $C_d = 0.2$ | $C_d = 0.5$ | $C_d = 1.0$ |
| $\beta = 0.2$ | n=1 | n=1 | n=1 | n=1 | n=1 | n=1 |
| $\beta = 0.5$ | n=1 | n=1 | n=1 | n=1 | n=1 | n=1 |
| $\beta = 0.7$ | n=1 | n=1 | n=1 | n=1 | n=1 | n=1 |

**Table A.2:Solutions for $D = 3m$ using $DU/Dt = \partial U/\partial t$**

| H=5 m | | | | | | |
|---|---|---|---|---|---|---|
| | d=100 m | | | d=500 m | | |
| parameters | $C_d = 0.2$ | $C_d = 0.5$ | $C_d = 1.0$ | $C_d = 0.2$ | $C_d = 0.5$ | $C_d = 1.0$ |
| $\beta = 0.2$ | n=1 | n=1 | n=1 | n=1 | n=1 | n=1 |
| $\beta = 0.5$ | n=1 | n=1 | n=1 | n=1 | n=1 | n=1 |
| $\beta = 0.7$ | n=1 | n=1 | n=1 | n=1 | n=1 | n=1 |

| H=10 m | | | | | | |
|---|---|---|---|---|---|---|
| | d=100 m | | | d=500 m | | |
| parameters | $C_d = 0.2$ | $C_d = 0.5$ | $C_d = 1.0$ | $C_d = 0.2$ | $C_d = 0.5$ | $C_d = 1.0$ |
| $\beta = 0.2$ | n=1 | n=1 | n=1 | n=1 | n=1 | n=1 |
| $\beta = 0.5$ | n=1 | n=1 | n=1 | n=1 | n=1 | n=1 |
| $\beta = 0.7$ | n=1 | n=1 | n=1 | n=1 | n=1 | n=1 |

| H=20 m | | | | | | |
|---|---|---|---|---|---|---|
| | d=100 m | | | d=500 m | | |
| parameters | $C_d = 0.2$ | $C_d = 0.5$ | $C_d = 1.0$ | $C_d = 0.2$ | $C_d = 0.5$ | $C_d = 1.0$ |
| $\beta = 0.2$ | n=1 | n=1 | n=1 | n=1 | n=1 | n=1 |
| $\beta = 0.5$ | n=1 | n=1 | n=1 | n=1 | n=1 | n=1 |
| $\beta = 0.7$ | n=1 | n=1 | n=1 | n=1 | n=1 | n=1 |

| H=30 m | | | | | | |
|---|---|---|---|---|---|---|
| | d=100 m | | | d=500 m | | |
| parameters | $C_d = 0.2$ | $C_d = 0.5$ | $C_d = 1.0$ | $C_d = 0.2$ | $C_d = 0.5$ | $C_d = 1.0$ |
| $\beta = 0.2$ | n=1 | n=1 | n=1 | n=1 | n=1 | n=1 |
| $\beta = 0.5$ | n=1 | n=1 | n=1 | n=1 | n=1 | n=1 |
| $\beta = 0.7$ | n=1 | n=1 | n=1 | n=1 | n=1 | n=1 |

**Table A.3:Solutions for $D = 1m$ using $DU/Dt = \partial U/\partial t$**

| H=5 m | | | | | | |
|---|---|---|---|---|---|---|
| d=100 m | | | | | | |
| parameters | $C_d = 0.2$ | | $C_d = 0.5$ | | $C_d = 1.0$ | |
| $\beta = 0.2$ | n=1 | | n=1 | | n=1 | |
| $\beta = 0.5$ | n=1 | | n=1 | | n=1 | |
| $\beta = 0.7$ | n=1 | | n=1 | | n=1 | |

| H=10 m | | | | | | |
|---|---|---|---|---|---|---|
| | d=100 m | | | d=500 m | | |
| parameters | $C_d = 0.2$ | $C_d = 0.5$ | $C_d = 1.0$ | $C_d = 0.2$ | $C_d = 0.5$ | $C_d = 1.0$ |
| $\beta = 0.2$ | n=1 | n=1 | n=1 | n=1 | n=1 | n=1 |
| $\beta = 0.5$ | n=1 | n=1 | n=1 | n=1 | n=1 | n=1 |
| $\beta = 0.7$ | n=1 | n=1 | n=1 | n=1 | n=1 | n=1 |

| H=20 m | | | | | | |
|---|---|---|---|---|---|---|
| | d=100 m | | | d=500 m | | |
| parameters | $C_d = 0.2$ | $C_d = 0.5$ | $C_d = 1.0$ | $C_d = 0.2$ | $C_d = 0.5$ | $C_d = 1.0$ |
| $\beta = 0.2$ | n=1 | n=1 | n=1 | n=1 | n=1 | n=1 |
| $\beta = 0.5$ | n=1 | n=1 | n=1 | n=1 | n=1 | n=1 |
| $\beta = 0.7$ | n=1 | n=1 | n=1 | n=1 | n=1 | n=1 |

| H=30 m | | | | | | |
|---|---|---|---|---|---|---|
| | d=100 m | | | d=500 m | | |
| parameters | $C_d = 0.2$ | $C_d = 0.5$ | $C_d = 1.0$ | $C_d = 0.2$ | $C_d = 0.5$ | $C_d = 1.0$ |
| $\beta = 0.2$ | n=1 | n=1 | n=1 | n=1 | n=1 | n=1 |
| $\beta = 0.5$ | n=1 | n=1 | n=1 | n=1 | n=1 | n=1 |
| $\beta = 0.7$ | n=1 | n=1 | n=1 | n=1 | n=1 | n=1 |

# Appendix B

# Numerical Calculation of the Largest Liapunov Exponent

This appendix contains a description of the method for the numerical calculation of the largest Liapunov exponent for a set of first order time dependent differential system. The algorithm here follows that given by Wolf et al. [36] and Moon [5].

## B.1 Definition

For an n-dimensional time-dependent differential system, we monitor the long term evolution of an infinitesimal n-sphere of initial conditions. The sphere will become an n-ellipsoid due to the local deformation. If $d_i(t)$ denotes the length of the $i^{th}$ ellipsoidal principal axis, then the $i^{th}$ Liapunov exponent is defined as (see for example, Wolf et al. [36]),

$$\lambda_i = \lim_{t\to\infty} \frac{1}{(t-t_0)} \ln \frac{d_i(t)}{d_i(t_0)}. \tag{B.1}$$

The $\lambda_i$, $i = 1, 2, \ldots, n$, ordered from largest to smallest, are related to the stretching and contracting nature of different directions in phase space. If $d(t)$ denotes the

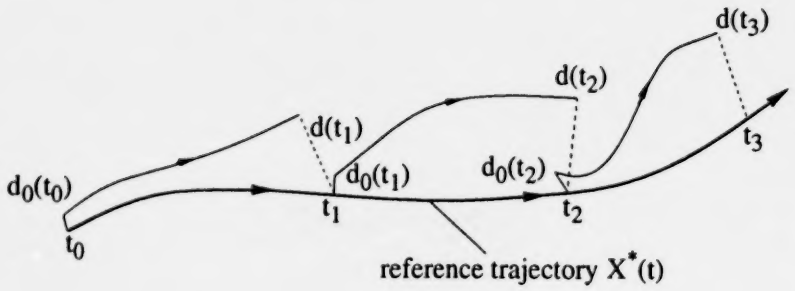


**Figure B.1:** Calculation of the largest Liapunov exponent form time series

largest length of ellipsoidal principal axis, the largest Liapunov exponent is then defined as

$$\lambda_1 = \lim_{t\to\infty} \frac{1}{(t-t_0)} \ln \frac{d(t)}{d(t_0)} \tag{B.2}$$

A problem arises for using this definition directly to calculate $\lambda_1$. The divergence of chaotic trajectories can only be locally exponential as $d(t)$ cannot go to infinity if the system is bounded as is the case for a dissipative system, such as the articulated tower system discussed in this thesis. In practice, to obtain a measure of this divergence, averaging must be used to estimate the exponential growth at many points along a reference trajectory as shown in Figure B.1. Thus the procedure to measure this divergence of trajectories goes as follows. Beginning with a reference trajectory and a point on a nearby trajectory, measure $d(t)/d(0)$. When $d(t)$ grows too large, take a new "nearby" trajectory and define a new $d(0)$. In Equation B.2, let $t - t_0 = \tau$, and take $N$ samples. After averaging we have

$$\lambda_1 = \frac{1}{N} \sum_{i=1}^{N} \frac{1}{\tau} \ln \frac{d(t_i)}{d_0(t_{i-1})}$$

$$= \frac{1}{N\tau}\sum_{i=1}^{N}\frac{d(t_i)}{d_0(t_{i-1})}$$

$$= \frac{1}{t_N - t_0}\sum_{i=1}^{N}\frac{d(t_i)}{d_0(t_{i-1})}. \tag{B.3}$$

It can be seen that the main idea to calculate $\lambda_1$ is to be able to determine the ratio $d(t_i)/d_0(t_{i-1})$.

## B.2 Algorithm for Computing the Largest Liapunov Exponent $\lambda_1$

The method described below to compute the largest Liapunov exponent follows that given in [5]. For a set of first order n-dimensional differential equations of the form

$$\dot{\mathbf{x}} = \mathbf{f}(\mathbf{x}, t), \tag{B.4}$$

integration gives a reference solution $\mathbf{x}^*(t)$. The integrating time should be long enough to get rid of the transients. Then take $\mathbf{x}^*(t_k)$ and a nearby point $\mathbf{x}^*(t_k) + \Delta\mathbf{x}(t_k)$ as initial conditions, where $\Delta\mathbf{x}(t_k)$ is the initial divergence vector with each component along each principal axis and can be obtained by solving the following variational equations.

Substitute $\mathbf{x}^*(t_k) + \Delta\mathbf{x}(t_k)$ into Equation B.4 to get

$$\dot{\mathbf{x}}^*(t_k) + \Delta\dot{\mathbf{x}}(t_k) = \mathbf{f}(\mathbf{x}^* + \Delta\mathbf{x}, t). \tag{B.5}$$

Expanding $\mathbf{f}(\mathbf{x}^* + \Delta\mathbf{x}, t)$ in Taylor series in the vicinity of $\mathbf{x}^*(t_k)$ and retaining the linear terms, we have

$$\Delta\dot{\mathbf{x}}(t_k) = \left.\frac{\partial \mathbf{f}}{\partial \mathbf{x}}\right|_{\mathbf{x}=\mathbf{x}^*} \Delta\mathbf{x}(t_k) \tag{B.6}$$

or

$$\Delta\dot{\mathbf{x}}(t_k) \;=\; \mathbf{J}|_{\mathbf{x}=\mathbf{x}^*}\,\Delta\mathbf{x}(t_k) \tag{B.7}$$

where $\partial\mathbf{f}/\partial\mathbf{x}|_{\mathbf{x}=\mathbf{x}^*} = \mathbf{J}$ is the Jacobian matrix evaluated at $\mathbf{x} = \mathbf{x}^*$. Equation B.7 is called variational equations, and it represents the linearization of vector field along a trajectory. Thus at each time step, called the Liapunov time step, $\tau = t_{k+1} - t_k$ should be small to minimize the error.

In practice, we can integrate Equations B.4 and B.7 simultaneously, taking into account the change in $\mathbf{J}$ through $\mathbf{x}^*(t)$. After a given time interval $\tau = t_{k+1} - t_k$, take

$$\frac{d(t_{k+1})}{d(t_k)} \;=\; \left|\frac{\Delta\mathbf{x}(\tau, t_k)}{\Delta\mathbf{x}(0, t_k)}\right|. \tag{B.8}$$

For next step, use the direction of $\Delta\mathbf{x}(\tau, t_k)$ and normalize it to get

$$\Delta\mathbf{x}(0, t_{k+1}) \;=\; \frac{\Delta\mathbf{x}(\tau, t_k)}{|\Delta\mathbf{x}(0, t_k)|}. \tag{B.9}$$